



**UNIVERSIDAD DE INVESTIGACIÓN DE TECNOLOGIA
EXPERIMENTAL YACHAY**

Escuela de Ciencias Biológicas e Ingeniería

**TITULO: SYNTHESIS OF BIOFUNCTIONAL
POLYTETRAFLUOROETHYLENE NANOPARTICLES FOR
THE DUAL X-RAY AND ULTRASOUND BIOIMAGING**

Trabajo de Integración curricular presentado como requisito para la
obtención del título de Ingeniero Biomédico

Autor:

Dilan Andrés Quinchiguango Pérez

Tutor:

PhD. Frank Alexis

Urcuquí, agosto, 2021

Urcuquí, 4 de agosto de 2021

SECRETARÍA GENERAL
(Vicerrectorado Académico/Cancillería)
ESCUELA DE CIENCIAS BIOLÓGICAS E INGENIERÍA
CARRERA DE BIOMEDICINA
ACTA DE DEFENSA No. UITEY-BIO-2021-00028-AD

A los 4 días del mes de agosto de 2021, a las 11:30 horas, de manera virtual mediante videoconferencia, y ante el Tribunal Calificador, integrado por los docentes:

| | |
|---------------------------------------|--|
| Presidente Tribunal de Defensa | Dr. SANTIAGO VISPO, NELSON FRANCISCO , Ph.D. |
| Miembro No Tutor | Dr. SINCHE CHELE, FEDERICO LEONARDO , Ph.D. |
| Tutor | Dr. ALEXIS FRANK , Ph.D. |

El(la) señor(ita) estudiante **QUINCHIGUANGO PEREZ, DILAN ANDRES**, con cédula de identidad No. **0401864160**, de la **ESCUELA DE CIENCIAS BIOLÓGICAS E INGENIERÍA**, de la Carrera de **BIOMEDICINA**, aprobada por el Consejo de Educación Superior (CES), mediante Resolución **RPC-SO-43-No.496-2014**, realiza a través de videoconferencia, la sustentación de su trabajo de titulación denominado: **SYNTHESIS OF BIOFUNCTIONAL POLYTETRAFLUOROETHYLENE NANOPARTICLES FOR THE DUAL X-RAY AND ULTRASOUND BIOIMAGING**, previa a la obtención del título de **INGENIERO/A BIOMÉDICO/A**.

El citado trabajo de titulación, fue debidamente aprobado por el(los) docente(s):

| | |
|--------------|--------------------------|
| Tutor | Dr. ALEXIS FRANK , Ph.D. |
|--------------|--------------------------|

Y recibió las observaciones de los otros miembros del Tribunal Calificador, las mismas que han sido incorporadas por el(la) estudiante.

Previamente cumplidos los requisitos legales y reglamentarios, el trabajo de titulación fue sustentado por el(la) estudiante y examinado por los miembros del Tribunal Calificador. Escuchada la sustentación del trabajo de titulación a través de videoconferencia, que integró la exposición de el(la) estudiante sobre el contenido de la misma y las preguntas formuladas por los miembros del Tribunal, se califica la sustentación del trabajo de titulación con las siguientes calificaciones:

| Tipo | Docente | Calificación |
|--------------------------------|--|---------------------|
| Tutor | Dr. ALEXIS FRANK , Ph.D. | 10,0 |
| Miembro Tribunal De Defensa | Dr. SINCHE CHELE, FEDERICO LEONARDO , Ph.D. | 10,0 |
| Presidente Tribunal De Defensa | Dr. SANTIAGO VISPO, NELSON FRANCISCO , Ph.D. | 10,0 |

Lo que da un promedio de: **10 (Diez punto Cero)**, sobre 10 (diez), equivalente a: **APROBADO**

Para constancia de lo actuado, firman los miembros del Tribunal Calificador, el/la estudiante y el/la secretario ad-hoc.

Certifico que *en cumplimiento del Decreto Ejecutivo 1017 de 16 de marzo de 2020, la defensa de trabajo de titulación (o examen de grado modalidad teórico práctica) se realizó vía virtual, por lo que las firmas de los miembros del Tribunal de Defensa de Grado, constan en forma digital.*



QUINCHIGUANGO PEREZ, DILAN ANDRES

Estudiante

NELSON FRANCISCO
 FRANCISCO
 SANTIAGO VISPO
 SANTIAGO VISPO

Firmado digitalmente por
 NELSON FRANCISCO
 SANTIAGO VISPO
 Fecha: 2021.08.04 12:32:00
 -05'00'

Dr. SANTIAGO VISPO, NELSON FRANCISCO , Ph.D.

Presidente Tribunal de Defensa



Firmado digitalmente por
FRANK ALEXIS

Dr. ALEXIS FRANK , Ph.D.
Tutor



Firmado digitalmente por
**FEDERICO
LEONARDO SINCHE
CHELE**

Dr. SINCHE CHELE, FEDERICO LEONARDO , Ph.D.

Miembro No Tutor

**KARLA ESTEFANIA
ALARCON FELIX**

Firmado digitalmente por KARLA
ESTEFANIA ALARCON FELIX
Fecha: 2021.08.04 12:42:17 -05'00'

ALARCON FELIX, KARLA ESTEFANIA
Secretario Ad-hoc

AUTORÍA

Yo, **DILAN ANDRÉS QUINCHIGUANGO PÉREZ**, con cédula de identidad **0401864160** declaro que las ideas, juicios, valoraciones, interpretaciones, consultas bibliográficas, definiciones y conceptualizaciones expuestas en el presente trabajo; así como, los procedimientos y herramientas utilizadas en la investigación, son de absoluta responsabilidad de el/la autora (a) del trabajo de integración curricular. Así mismo, me acojo a los reglamentos internos de la Universidad de Investigación de Tecnología Experimental Yachay.

Urcuquí, agosto, 2021.



Dilan Andrés Quinchiguango Pérez

CI: 0401864160

AUTORIZACIÓN DE PUBLICACIÓN

Yo, **DILAN ANDRÉS QUINCHIGUANGO PÉREZ**, con cédula de identidad **0401864160**, cedo a la Universidad de Tecnología Experimental Yachay, los derechos de publicación de la presente obra, sin que deba haber un reconocimiento económico por este concepto. Declaro además que el texto del presente trabajo de titulación no podrá ser cedido a ninguna empresa editorial para su publicación u otros fines, sin contar previamente con la autorización escrita de la Universidad.

Asimismo, autorizo a la Universidad que realice la digitalización y publicación de este trabajo de integración curricular en el repositorio virtual, de conformidad a lo dispuesto en el Art. 144 de la Ley Orgánica de Educación Superior

Urcuquí, agosto, 2021.



Dilan Andrés Quinchiguango Pérez

CI: 0401864160

DEDICATORIA

Dedico el presente trabajo a mi familia, amigos y cada una de las personas que me han apoyado incondicionalmente de una u otra manera y sin duda alguna han sido parte fundamental para el inicio de esta nueva etapa profesional.

En especial dedico esta tesis con mucho amor a mis padres Narciza Pérez y Angel Quinchiguango por haberme forjado como la persona que soy en la actualidad, muchos de mis logros se los debo a ustedes entre los que se incluye este. Mi padre por ser un hombre correcto y paciente que me ha guiado siempre a tomar las mejores decisiones. Mi madre que ha sido la parte más importante en mi vida, la mujer que más amo en este mundo, pues sin ella no lo habría logrado. Por su esfuerzo y sacrificio que hoy me permite obtener un título profesional.

Gracias a todos.

Dilan Andrés Quinchiguango Pérez

Agradecimiento

En primer lugar, me gustaría agradecer de manera especial y sincera a Ph.D. Si Amar Dahoumane por el invaluable apoyo brindado durante la realización de este proyecto de tesis, por compartir sus conocimientos, la motivación brindada en cada paso, ser un gran maestro y amigo. Además, mi agradecimiento a mi asesor Ph.D. Frank Alexis, cuyo acompañamiento, paciencia y experiencia han sido fundamentales en este proyecto. Además, agradezco a los profesores Ph.D. Carlos Reinoso, Ph.D. Edward Ávila y Ph.D. Terencio Thibault por su apoyo en el proceso de caracterización de la muestra. También agradezco a la Ing. Paola Echeverría, técnica de laboratorio, por su consejos y ayuda incondicional, que me permitió realizar las pruebas de laboratorio. En ESPE (Sangolquí, Ecuador) agradezco a Karla Vizuite y Alexis Debut por ayudarme a obtener los resultados finales. Finalmente, mi eterna gratitud a mis padres, familiares y amigos que siempre me motivaron a seguir adelante, cumplir metas y hoy hacen posible la obtención de mi título universitario.

Dilan Andrés Quinchiguango Pérez

CONTENTS

| | |
|---|------------|
| Resumen..... | XI |
| Abstract..... | XII |
| 1. INTRODUCTION | 1 |
| 1.1 Literature Review..... | 1 |
| 1.1.1 What is PTFE? | 1 |
| 1.1.2 Cancer | 5 |
| 1.1.3 Current Cancer Treatments | 8 |
| 1.1.4 Nanomaterials | 13 |
| 1.1.5 Nanoparticles and Cancer | 17 |
| 1.1.6 Nanoparticles and Bioimaging..... | 20 |
| 1.2 Problem Statement | 27 |
| 1.3 General and Specific Objectives | 29 |
| 2. METHODOLOGY | 30 |
| 2.1 Synthesis of PTFE Fine-powder. | 30 |
| 2.2 Production of PTFE Nanoparticles | 32 |
| 2.2.1 Sonication | 32 |
| 2.3 Characterization Techniques..... | 34 |
| 2.3.1 X-ray Diffraction..... | 34 |
| 2.3.2 Scanning Electron Microscopy | 36 |
| 2.3.3 Transmission Electron Microscopy | 37 |
| 2.3.4 UV–Vis analysis | 38 |
| 2.3.5. X-ray Photoelectron Spectroscopy (XPS)..... | 39 |
| 3. RESULTS & DISCUSSION | 41 |
| 3.1 Characterization | 41 |
| 3.1.1 Diffuse Reflectance UV-Vis Analysis (PTFE Fine-powder)..... | 41 |
| 3.1.2 X-ray Diffraction (PTFE Powder) | 45 |
| 3.1.3 X-ray Photoelectron Spectroscopy (XPS)..... | 53 |
| 3.1.4 Transmission Electron Microscopy (TEM - PTFE NPS) | 56 |
| 4. CONCLUSIONS & OUTLOOK..... | 59 |

| | |
|--------------------------|-----------|
| 4.1 Conclusion | 59 |
| 4.2 Outlook | 59 |
| A1 Abbreviations | 61 |
| BIBLIOGRAPHY..... | 63 |

List of Tables

| | |
|---|----|
| Table 1.1. Summary of the main physicochemical properties of PTFE. | 3 |
| Table 1.2. Types of energy release depending on the location and anatomical position of the tumor. | 11 |
| Table 1.3 Advantages and disadvantages of the application of X-rays in clinical practice. | 23 |
| Table 1.4. Advantages and disadvantages of ultrasound as an imaging system | 25 |
| Table 3.1 Miller Indices, interplanar distances, and peak location calculated from XRD pattern | 48 |
| Table 3.2. Full-Width at a half maximum (FWHM) values calculated from the PTFE X-ray diffraction pattern..... | 51 |
| Table 3.3. Summary of the parameters calculated from the PTFE diffraction pattern. | 53 |
| Table 3.4. Atomic percentage and binding energies of the elements that compose PTFE..... | 54 |

List of figures

| | |
|---|----|
| Figure 1.1 Phase IV PTFE helical structure composed of 15/atoms turn | 1 |
| Figure 1.2. Schematic representation of the TFE synthesis process and polymerization methodology to obtain commercial PTFE. | 2 |
| Figure 1.3. Medical devices made of PTFE. | 5 |
| Figure 1.4. Cancer formation process through genetic mutation in DNA repair mechanisms | 6 |
| Figure 1.5. Cancer statistics in Ecuador, 2020. | 7 |
| Figure 1.6. Hyperthermia working principle for tumor destruction. | 10 |
| Figure 1.7. Heat generated in tissues and temperature measurement in hyperthermia treatment of cancer. | 11 |
| Figure 1.8. Photothermal therapy mechanism of action. | 12 |
| Figure 1.9. Classification of Nanostructured materials (0D, 1D, 2D, 3D) with their corresponding shape and size. | 15 |
| Figure 1.10. Schematic representation of the Particle Replication In Non-wetting Templates technology process. | 17 |
| Figure 1.11. Graphical representation of nanoplatforms used as drug delivery systems for cancer treatment and other diseases. | 19 |
| Figure 1.12. Chemical structure of contrast agents employed to improve X-ray bioimaging. | 21 |
| Figure 1.13. PTFE felt pledgets | 22 |
| Figure 1.14. Computed tomography image after 3h and 120h of intravenous injection of iodinated polyvinyl alcohol nanoparticles | 23 |

| | |
|---|----|
| Figure 1.15. Nanobubble composed of a polymeric shell enclosing the core composed of C ₃ F ₈ gas. | 24 |
| Figure 1.16 Ultrasound contrast agent composed of a lipid shell (PLA) loaded with gold nanorods to imaging the kidney vasculature. | 25 |
| Figure 2.1. Graphic description of the PTFE fine-powder synthesis process..... | 31 |
| Figure 2.2 Ultrasonic fragmentation process. | 33 |
| Figure 2.3. Working principle of X-ray diffraction. | 35 |
| Figure 2.4. Schematic description of the image obtention process and chamber components of Scanning Electron Microscopy. | 37 |
| Figure 2.5. Transmission Electron Microscopy system for image obtainment. | 38 |
| Figure 2.6. Diagram of the photoelectric effect that governs the XPS technique..... | 40 |
| Figure 3.1. Diffuse Reflectance Spectroscopy spectra of PTFE fine powder and Kubelka-Munk transformation..... | 42 |
| Figure 3.2. Diffraction patterns of PTFE. | 46 |
| Figure 3.3. Unit cell and diffraction planes of PTFE..... | 50 |
| Figure 3.4. Factors that influence the Scherrer equation to calculate the crystallite size utilizing the x-ray diffraction pattern. | 52 |
| Figure 3.5. XPS survey spectrum of PTFE..... | 54 |
| Figure 3.6. High-resolution survey spectrum and peak deconvolution of PTFE..... | 55 |
| Figure 3.7. Transmission electron Microscopy micrograph of PTFE NPs..... | 57 |
| Figure 3.8. Particle size distribution. | 57 |

Resumen

El politetrafluoroetileno (PTFE) exhibe propiedades únicas y fascinantes, como inercia química, alta estabilidad mecánica, estructura hidrófoba, alta resistencia eléctrica y estabilidad térmica. Estas cualidades hacen de este material un candidato ideal en los campos emergentes de la bioingeniería, como la ingeniería de tejidos, los injertos vasculares y los recubrimientos de implantes. Un proyecto de tesis realizado en la Universidad Tecnológica de Yachay (2018-2019) confirmó que el polvo de PTFE absorbe ultrasonidos y rayos X, demostrando su capacidad como agente de contraste para aplicaciones de bioimagen. El presente trabajo tiene como objetivo sintetizar nanopartículas (NP) a partir de PTFE de alta pureza, caracterizar sus características (forma, tamaño, cristalinidad, pureza y composición) para su uso en bioimagen y, en última instancia, en el tratamiento de la hipertermia del cáncer. Se utilizaron varias técnicas para caracterizar completamente las nanopartículas de PTFE obtenidas desde un punto de vista físico-químico. Las imágenes de microscopía electrónica de transmisión mostraron nanopartículas de PTFE esféricas y en forma de varilla con un tamaño promedio de 70 nm. La espectroscopía UV-Visible determinó que el PTFE absorbe hasta el 90% de la radiación electromagnética en la región ultravioleta y actúa como material aislante (3,125 eV). Se utilizó difracción de rayos X para examinar primero la composición química del polvo fino, demostrando la ausencia de contaminantes inorgánicos. En segundo lugar, reveló que la muestra de nanopartículas de PTFE es altamente cristalina (85%). Asimismo, la espectroscopia fotoelectrónica de rayos X (XPS) confirmó la ausencia de contaminantes inorgánicos y cuantificó el porcentaje de elementos que componen la muestra. El trabajo futuro evaluará primero la biocompatibilidad de estas nanopartículas de PTFE puro libres de contaminantes. Luego, se investigará su potencial como agente de contraste versátil bajo rayos X e irradiación de ultrasonido. Finalmente, el trabajo posterior explorará su promesa en la teranóstica del cáncer.

Palabras clave: Politetrafluoroetileno, PTFE, nanopartículas, cáncer, bioimagen, agentes de contraste, técnicas de caracterización, análisis UV-VIS, análisis XRD, patrón XPS, TEM.

Abstract

Polytetrafluoroethylene (PTFE) exhibits unique and fascinating properties, such as chemical inertness, high mechanical stability, hydrophobic structure, high electrical resistance, and thermal stability. These qualities make this material an ideal candidate in emerging fields of bioengineering, such as tissue engineering, vascular grafts, and implant coatings. A thesis project carried out at Yachay Tech University (2018-2019) confirmed that PTFE powder absorbs ultrasound and X-rays, demonstrating its ability as a contrast agent for bioimaging applications. The present work aims to synthesize nanoparticles (NPs) from high purity PTFE, characterize its characteristics (shape, size, crystallinity, purity, and composition) towards its use in bioimaging and, ultimately, in the hyperthermia treatment of cancer. Several techniques were used to fully characterize the obtained PTFE nanoparticles from a physico-chemical point-of-view. Transmission electron microscopy images showed spherical and rod-shaped PTFE nanoparticles with an average size of 70 nm. UV-Visible spectroscopy determined that PTFE absorbs up to 90% of the electromagnetic radiation in the ultraviolet region and acts as an insulating material (3.125 eV). X-ray diffraction was used to first examine the chemical composition of the fine powder, demonstrating the absence of inorganic contaminants. Second, it revealed that the PTFE nanoparticles sample is highly crystalline (85%). Likewise, X-ray photoelectron spectroscopy (XPS) confirmed the absence of any inorganic contaminants and quantified the percentage of elements that make up the sample. Future work will first evaluate the biocompatibility of these pure PTFE nanoparticles free of any contaminants. Then, their potential as a versatile contrast agent under X-rays and ultrasound irradiation will be investigated. Finally, subsequent work will explore their promise in cancer theranostics.

Key words: Polytetrafluoroethylene, PTFE, nanoparticles, cancer, bioimaging, contrast agents, characterization techniques, UV-VIS analysis, XRD analysis, XPS pattern, TEM.

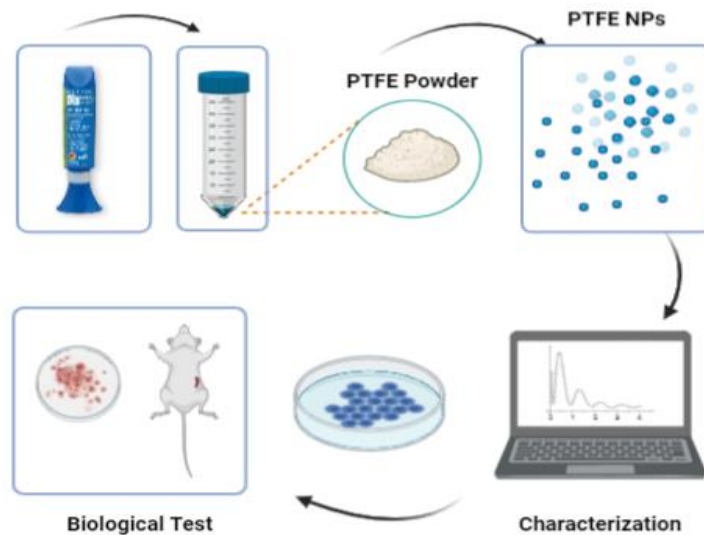


Figure 0. Graphical description of the procedure carried out since the synthesis to the biological test of PTFE NPs including their physico-chemical characterization.

CHAPTER 1

INTRODUCTION

1.1 Literature Review

1.1.1 What is PTFE?

Polytetrafluoroethylene (PTFE) is a fluoro-synthetic polymer discovered in 1938 by Dr. Roy Plunkket at DuPont company while searching for safe fluorinated refrigerants. Its chemical structure comprises carbon backbone atoms covalently bound to fluorine atoms, which provides it unique properties such as chemical, mechanical and thermal stability. PTFE has a crystalline domain separated by amorphous regions that determine its semicrystalline structure and exists in 4 primary phases, phases 1 and 4 being the most common, as they exist at atmospheric pressure and room temperature. At room temperature, the PTFE has a hexagonal structure with 15 atoms/180-degree turn^{1,2} (**Figure 1.1**).

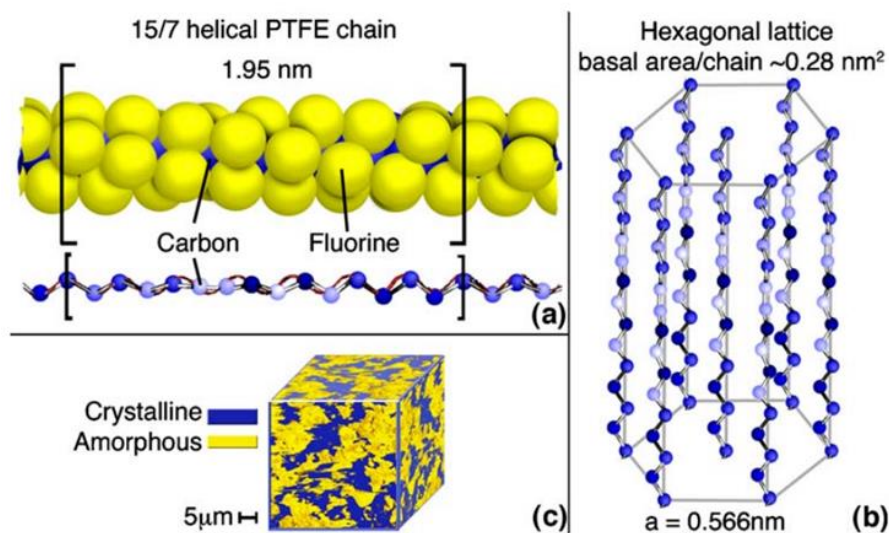


Figure 1.1. Crystallographic features of PTFE: (a) Phase IV PTFE helical structure composed of 15 atoms/turn. (b) Hexagonal crystal lattice spacing. (c) PTFE crystalline and amorphous domains. Source: Brown et al. (2008).

Synthesis

The manufacturing of commercial PTFE begins with the synthesis of tetrafluoroethylene (TFE) monomer, a colorless, odorless and highly flammable gas. In the literature, the synthesis techniques of TFE varies; however, the ultrafast pyrolysis of chlorodifluoromethane, ultrafast plasma pyrolysis of tetrafluoromethane, pyrolysis of chlorodifluoromethane (CHClF_2), dechlorination of $\text{CF}_2\text{Cl}-\text{CF}_2\text{Cl}$ are the most adopted and accepted in the scientific community.³ After obtaining the building brick, the next step consists in polymerizing the monomer to obtain the PTFE. The dispersion or emulsion polymerization method is the most widely used and takes place in high-pressure equipment under strictly controlled laboratory conditions. Commercial production is carried out in large, high pressure, stirred-tank reactors.³ In this procedure, the TFE gets in contact with soluble water, a dispersion agent, an anticoagulant, pH buffers, and chemical technical assistants (CTAs) to obtain a polymeric suspension.³ This methodology, known as "semi-batch process," involves adding reagents directly to the reactor while the reaction is taking place. No material is extracted from the reactor for the duration of the reaction. Finally, the PTFE fine-powder is washed and dried for later commercialization.^{3,4} **Figure 1.2** represents the PTFE synthesis process.

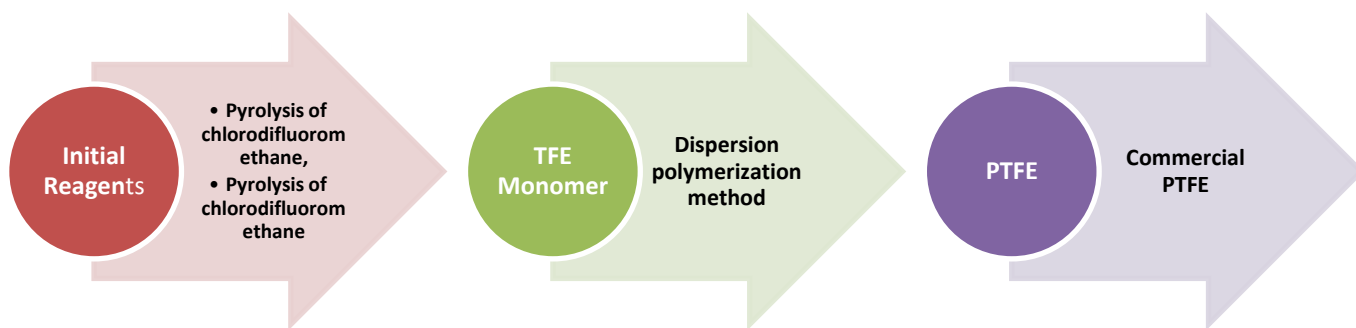


Figure 1.2. Schematic representation of the TFE synthesis process and polymerization methodology to obtain commercial PTFE.

Physicochemical Properties

The physicochemical properties of PTFE derive mainly from the nature of the C-F bond.⁵ This chemical bond is a covalent type and one of the strongest in organic chemistry; it has binding dissociation energy of $\sim 460 \text{ kJ mol}^{-1}$ and is the principal determining the thermal stability and chemical resistance of PTFE.³ Similarly, the molecular weight of PTFE ($\sim 10^6 - 10^7 \text{ g mol}^{-1}$), the length of the C-F bond and the size of the fluorine atom enclosing the carbon backbone make this polymer chemically inert to almost all solvents, whether acids or bases.^{2,3} Likewise, the high molecular weight generates a notably high melting point in a range of 300-330 °C.³ The crystalline structure and high molecular weight explain the mechanical properties of PTFE. Considering that the fluorine atom is large, it restricts the backbone movement, conceding an elongation capacity of $\sim 300\%$.^{2,3,5} Another essential feature is that PTFE is a hydrophobic material with a water contact angle of $\sim 118^\circ$.³ This property results from the low polarity of the PTFE chain that does not allow bonding with water through hydrogen bonds. This non-polarity of the chain provides the material with exceptional dielectric strength.³ Finally, PTFE has a tight helical structure in which the backbone remains rigid due to the repulsive forces of fluorine atoms. This chemical conformation determines its low coefficient of friction and low adhesion properties. **Table 1.1** summarizes all the physicochemical properties of PTFE.^{2,3}

Table 1.1. Summary of the main physicochemical properties of PTFE.

| Physicochemical Properties | Value |
|---------------------------------|------------------------------|
| Density | 2.2 – 2.3 g/cm ⁻³ |
| Water absorption, 24h | < 0.01 % |
| Dielectric constant at 1 kHz | 2.0 |
| Melting point | 335 °C |
| Dielectric constant | 2.0 |
| Dynamic coefficient of friction | 0.4 |
| Surface energy | 18 Dynes/g |
| Tensile strength | 31 MPa |
| Compressive strength | 4.4 MPa |

| | |
|-----------------------------|-------|
| Tensile elongation at break | 300 % |
| Hardness, shore D | D60 |

Biocompatibility

All the properties mentioned above make PTFE an exceptional material for use in biomedicine. In this sense, biocompatibility studies confirm that PTFE is a highly safe material for use in humans.⁶⁻¹⁰ For example, *in vitro* hemocompatibility tests have shown no hemolysis after direct blood contact with PTFE. The cytocompatibility results also demonstrated good cell viability after direct contact of PTFE with CPA-47 cells.⁶ Moreover, PTFE has excellent resistance against microorganisms and fungi since it does not generate an allergic immune response.^{7,8} The negatively charged surface of PTFE does not react with blood components; therefore, the body does not generate an allergic immune response.⁹ Finally, PTFE does not induce an alarming inflammatory response when implanted in subcutaneous tissue.¹⁰

Applications

Today, medicine and bio-engineering exploit the extraordinary physicochemical and biological properties of PTFE to design safe and biocompatible medical devices. **Figure 1.3.** presents some medical devices synthesized from PTFE. The Gore Medical Company (USA) is a pioneer in designing PTFE biomedical devices implanted in millions of patients per year worldwide.¹¹ In this context, PTFE vascular grafts are the most widely used medical devices in medicine for coronary artery bypass as hemodialysis access. Some vascular grafts are modified with pro-angiogenic molecules and heparin to minimize the blood clotting process and promote cell growth.¹² These vascular grafts do not require preclotting, are resistant to bacterial infections and have good mechanical stability.¹¹ Another product popularly employed in the medical field is the PTFE patch for abdominal wall hernia repair. When visceral adhesion is the main problem, the PTFE patch covers the injured area of the abdominal wall.¹³ Thus, the PTFE surface prevents the adhesion of visceral tissue. Also, this patch exhibits excellent suture retention while the patient's tissue heals. This structure also minimizes the biological response to foreign substances.¹⁴ Sutures made of

PTFE are also commonly used in heart diseases, such as mitral valve repair.¹⁵ Thanks to their biocompatibility, these sutures do not induce any adverse response in the tissues and have a low rate of inflammation; they are non-absorbable and are used in superficial skin wounds or internal environments that require greater mechanical strength, such as anastomosis of vascular grafts, mitral valve repair and laparoscopic ventral hernia repair.^{16,17}

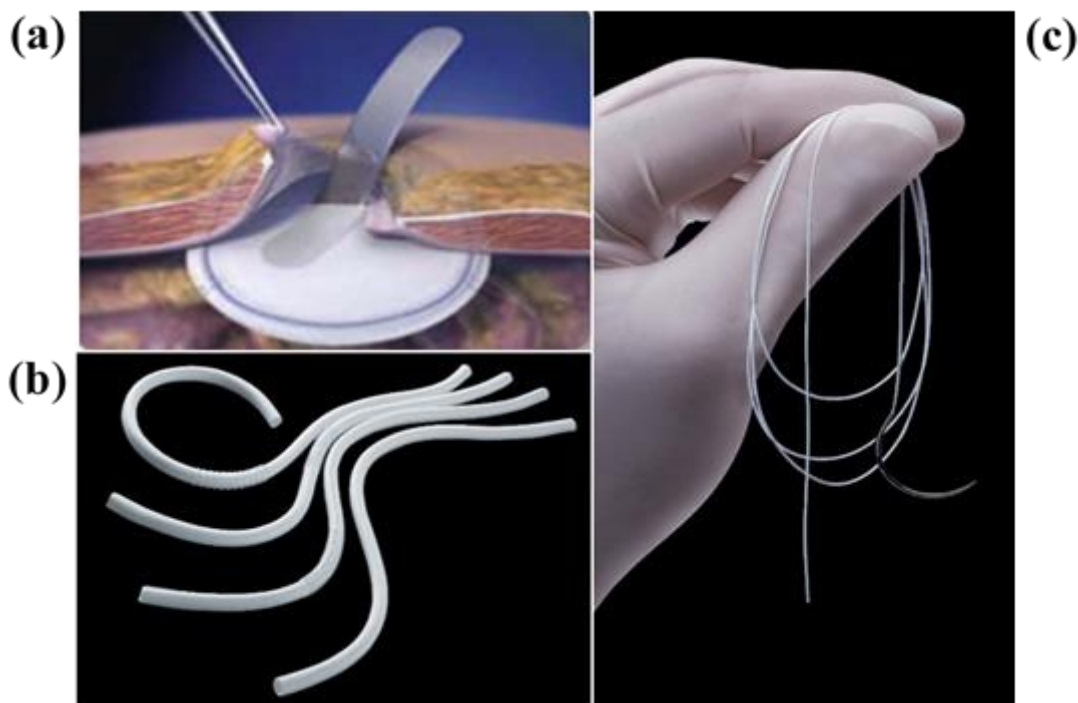


Figure 1.3. Medical devices made of PTFE. **(a)** PTFE patch used for abdominal hernia repair. **(b)** PTFE vascular grafts to coronary artery bypass. **(c)** PTFE sutures for internal and external environments. Source: Ebnesajjad (2016).

1.1.2 Cancer

Cancer is a disease that affects the cell cycle of normal cells in tissues.¹⁸ As can be seen in **Figure 1.4**, these affected cells begin a process of uncontrolled division, leading to tumors that can migrate to other tissues and metastasize. Additionally, cancer cells induce an angiogenesis process to create new blood vessels and obtain nutrients to sustain their growth in affected tissues.¹⁸ Genetic mutations, such as substitutions, deletions, translocations and insertions, can contribute to the onset of this disease. Basically, it is damage to the genetic material of cells.¹⁹ For example, colorectal hereditary nonpolyposis cancer results from mutations in the MLH1, MSH2, MSH6, PMS2, and

EPCAM genes responsible for DNA repair. Other scientific evidence shows that the affected genes BRCA1, BRCA2, PALB2, TP53, PTEN, and STK11 are responsible for breast cancer.²⁰ According to the World Health Organization (WHO), nutritional factors, uncontrolled addictions, and physical inactivity are the leading causes of cancer development. Low-income countries have the highest mortality rate of this disease as there are no early diagnosis systems to plan adequate early treatment. In 2018, 9.6 million deaths from cancer were reported worldwide.²¹

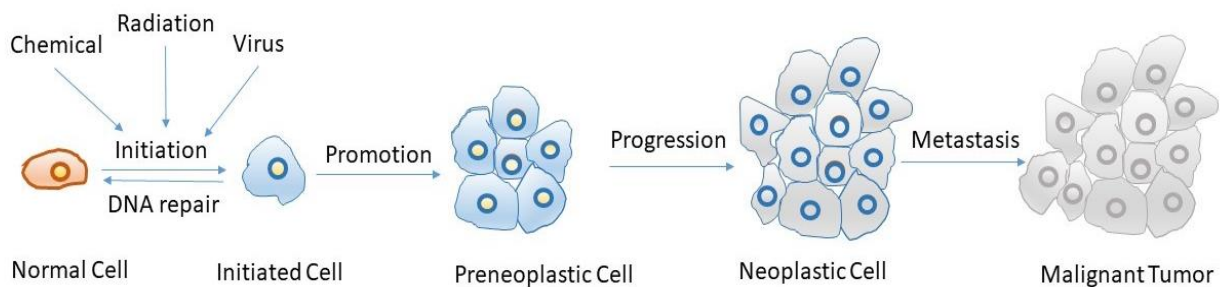


Figure 1.4. Cancer formation process through genetic mutation in DNA repair mechanisms that leads to uncontrolled cell division and subsequent metastasis. Source: APUS: Introduction to nutrition, (2020).

Cancer in Ecuador

According to the Global Cancer Observatory (GLOBOCAN)^{22,23}, ~29,000 new cancer cases were reported in Ecuador in 2020. From the total number of reported cases, breast cancer and prostate cancer have the highest incidence in female (12%) and male (11%) populations, respectively, as shown in **Figure 1.5**. Furthermore, 51% of patients die from this disease per year, and a total of 79,062 cases prevail in 5 years.²³

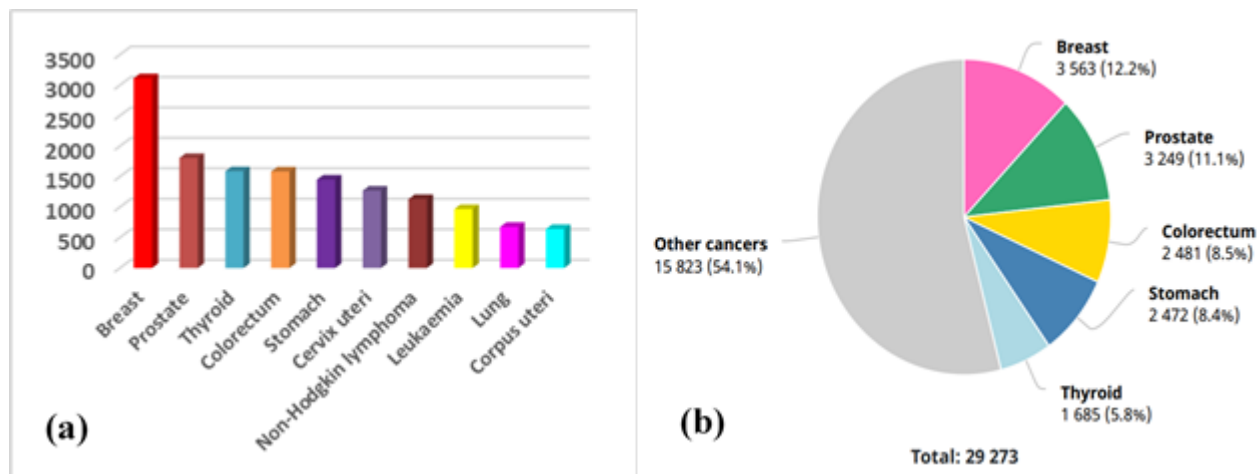


Figure 1.5. Cancer statistics in Ecuador for 2020. (a) Estimated number of incident cases Ecuador, both sexes, ages 0-74. (b) Percentage of the different types of cancer that affect the Ecuadorian population. Breast cancer and prostate cancer have a higher incidence in the female and male population respectively. Source: GLOBOCAN, 2020.

In order to comply with the resolutions on cancer prevention and control prepared by the National Health Assembly (2005), the Ecuadorian Ministry of Public Health (MSP), designed the National Strategy for Comprehensive Cancer Care (Estrategia Nacional de Atención Integral del Cáncer) for the early diagnosis of cancer, life quality improvement, reduction of the incidence, morbidity and mortality in people affected by this disease. In Ecuador, the Sociedad de Lucha contra el Cáncer (SOLCA) is responsible for processing and analyzing cancer's geographic incidence. According to MSP, first-level facilities are responsible for providing health prevention services, such as self-assessment counseling to detect breast cancer and a Papanicolaou service to prevent cervical cancer. Second-level facilities provide specialized ambulatory and hospitalization services. However, they do not have the technology to perform cancer detection tests; thus, patients are referred to third-level, highly specialized institutions to deal with their disease. In this sense, since the comprehensive public health network does not have services that can diagnose and treat cancer, it establishes agreements with private hospitals such as SOLCA. Despite the existence of the Instituto Nacional de Investigación en Salud Pública (INSPI), there is little research on cancer in Ecuador.²⁴

1.1.3 Current Cancer Treatments

Surgery

Surgery is one of the most used techniques to treat cancer. The procedure consists in removing the cancerous tissue from the affected organ. In Ecuador, several hospitals belonging to the private institution SOLCA, located in Guayaquil, Quito, Cuenca, Portoviejo and Loja, offer different programs to prevent, diagnose and treat cancer. In addition, SOLCA hospitals offer oncological surgery in the areas of gynecology, mastology, otorhinolaryngology, urology, neurology, head and neck surgery, bone tumor detection, skin, soft tissue and liver tumor detection. The surgery can be of two types:

- **Minimally invasive:** The surgeon makes a small incision near the affected area to insert a laparoscope that serves as an image guide to cut into the cancerous tissue and remove it from the body. The main advantage of this type of surgery consists in short recovery time. Surgery is used for solid tumors located in specific organs; it is not applied when metastasis has occurred. The objective is the complete or partial removal of the tumor to improve the patient's quality of life.²⁵
- **Open surgery:** The surgeon makes a large cut in the body when the tumor is in a hard-to-reach place. Recovery time is long and painful.²⁵

The most commonly used device in cancer surgery is the Da Vinci robot. There are around 4,900 robots around the world that have performed approximately 6 million surgeries.²⁶ However, new companies such as TransEnterix Inc (USA), and Cambridge Medical Robotics (UK) are developing minimally invasive devices.²⁶

Radiotherapy

Radiotherapy uses X-ray beams to damage the internal structure and genetic material of cancer cells. The medical device used for this treatment is the linear accelerator. The X-rays delivered to the patient are planned according to the type of tumor, its volume and anatomical location.²⁷ Radiation therapy is a local treatment, that is, the X-ray beam is directed to a specific area in the

body where the tumor is located.²⁷ In the same way, there is another type of radiotherapy called brachytherapy in which a radioactive device is inserted into the patient's body. The device emits radiation to the surrounding cancerous tissues and destroys them.²⁸ In Ecuador, Solca hospitals offer radiotherapy and brachytherapy services to cancer patients.

Chemotherapy

Chemotherapy consists in administering drugs to the patient to destroy cancer cells and prevent their abnormal growth. However, current chemotherapy drugs are not entirely convincing as they can destroy healthy tissue cells and cause side-effects, such as fatigue, diarrhea, hair loss, nausea and vomiting.²⁸ The drugs used in chemotherapy exert their activity by affecting the cell cycle of cancer cells, preventing their growth. However, they also affect healthy cells.²⁹

Targeted therapy

In this type of therapy, monoclonal antibodies are used to mark the antigens or proteins present on the membrane of tumor cells to be recognized by the immune system and subsequently destroyed. Some tumor markers prevent the abnormal growth by altering the cell signaling system and indicating the cell to stop dividing.³⁰ Other synthetically engineered antibodies inhibit the angiogenesis process to prevent the tumor from forming new blood vessels and obtaining nutrients.^{28,30} Some of these synthetic antibodies can be linked to drugs and radiation sources to enhance this therapy.³⁰ The SOLCA hospitals in Ecuador has this service available.

Hyperthermia

In the treatment known as hyperthermia, heat is generated in the area affected by cancer cells through an external source (**Figure 1.6**).³¹ Scientific data has shown that heat can denature some proteins and break the internal structure of cells. The hyperthermia treatment makes cancer cells more susceptible to other treatments, such as radiotherapy or chemotherapy. The energy sources used are ultrasounds, microwaves and radiofrequency.^{28,31}

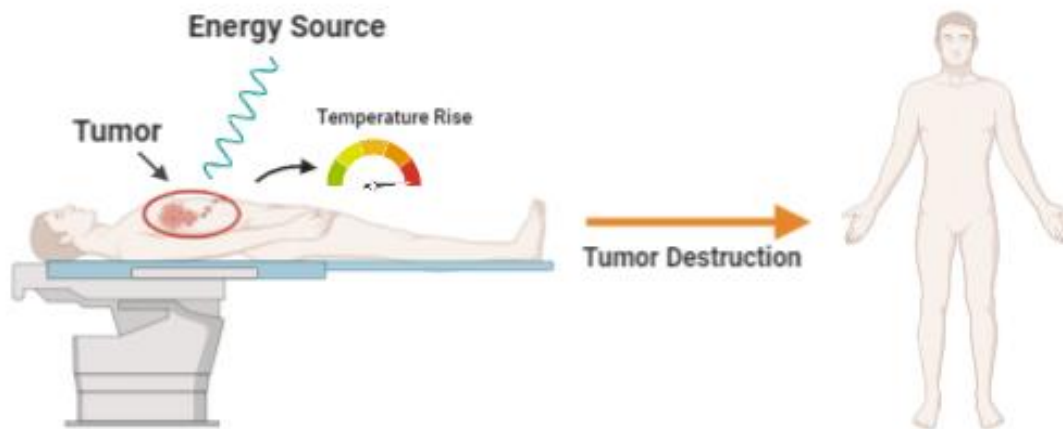


Figure 1.6. Hyperthermia working principle for tumor destruction.

Over the years, hyperthermia treatment of cancer has been gaining importance. The main limitations of this technique lie in the difficulty of accurately controlling the temperature of the affected and surrounding tissues when applying energy and imprecise techniques for heat generation to reach deep tissues.³² However, nanomaterials' development has opened new opportunities to initiate more effective and precise treatments against cancer. When tissues are subjected to heat through hyperthermia treatment, blood perfusion and oxygen increase, making tumor cells more susceptible to radiation therapy and drug delivery.^{32,33} **Figure 1.7** shows the temperature pattern obtained in tissues when heat is applied. For well-vascularized tumors, lower temperatures ($< 42\text{ }^{\circ}\text{C}$) and shorter time are used. Temperature below $42\text{ }^{\circ}\text{C}$ damages enzymes responsible for oxygen consumption, which leads to an oxygen accumulation in the tumor.³³ With temperatures higher than $42\text{ }^{\circ}\text{C}$, the tumor vasculature suffers damage, which causes a decrease in blood flow and oxygen, thus creating a more acidic environment and inducing protein denaturation and damage to DNA repair mechanisms.^{33,34} The heat and the duration of the therapy increase the rate of the cell death. Although the mechanism of hyperthermia in cells is unknown, there is evidence that cells in G_0 and S phases of the cell cycle have a greater sensitivity to this treatment.³⁴ Besides, the damage caused to the enzymes responsible for oxygen consumption causes the oxygen to concentrate with a greater quantity in the tumor cells, increasing the effectiveness of chemotherapy and radiation therapy. At temperatures around $45\text{ }^{\circ}\text{C}$, heat slows nucleic acid and

protein synthesis.³⁴ Additionally, when tumor cells enter hyperthermia, at the molecular level, the synthesis of heat shock proteins begins, associated with the cell's thermoresistance.³⁴ However, this treatment remains appropriate as tumor cells are less tolerant to heat.

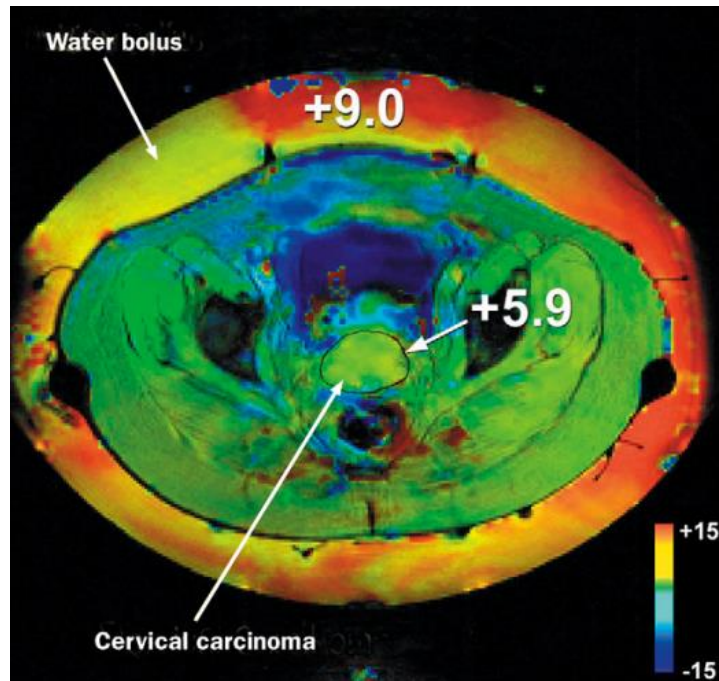


Figure 1.7. Heat generated in tissues and temperature measurement in hyperthermia treatment of cancer. Source: Wust. et al. (2002).

There are three types of hyperthermia³⁵:

- Local hyperthermia is applied in small areas of cancerous tissue to reach a maximum temperature of 45 °C. Heat is produced using radiofrequencies, ultrasounds or microwaves. Energy can be released in various ways depending on the location of the tumor. **Table 1.2.** presents the four types of energy release.

Table 1.2. Types of energy release depending on the location and anatomical position of the tumor.

| Types of energy release | Types of tumors |
|-------------------------|---------------------|
| External release | Subcutaneous tumors |

| | |
|-----------------------------|---|
| Intraluminal release | Tumors present in cavities, such as the esophagus and stomach. |
| Interstitial release | The energy applicators are inserted directly into the tumor. |
| Endocavitary release | Tumors present in hollow cavities, such as vagina, rectum, and esophagus. |

- Regional hyperthermia is used to treat big and deep tumors. Heat is applied using antennas or applicators around the areas of interest or by regional perfusion using fluids combined with drugs (chemotherapy). Are treated using this technique lung, liver, peritoneal and gastric cancers. In this treatment, the therapy lasts about 2 h and tissues are heated to about 43 °C. However, when fluids and chemotherapy are combined, treatment time and temperature are reduced.
- Full body hyperthermia involves warming the body to around 41 °C using anesthesia or sedation. This therapy is performed in hot water chambers, hot water blankets, hot wax or using infrareds. In combination with other therapies, temperatures of 40 °C are targeted.

Therefore, to improve conventional hyperthermia treatment, it has been identified that carbon-based nanomaterials reach a good conversion of light into heat for this type of therapy (**Figure 1.8**).³⁵

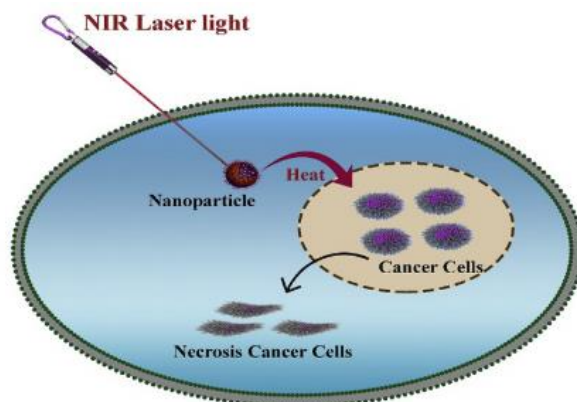


Figure 1.8. Photothermal therapy mechanism of action. Nanoparticles absorb light energy to generate heat and destroy cancer cells. Source: Elham Bridham, et al. (2019)

Nanoparticles and hyperthermia treatment of cancer

The surface modification of nanoparticles with ligands that recognize cancer cells is an excellent means to efficiently target cancer cells and solely act on these without damaging adjacent, healthy tissues. Similarly, these nanoplatfoms may act as drug carriers as they can be loaded with therapeutic agents to provide better and more specific treatments. Carbon nanotubes are among the most studied nanomaterials since they absorb a large amount of energy in the NIR and convert it into heat.³³ Evidence have shown that body enzymes can degrade organic photothermic agents; consequently, they do not exert any toxicity and are highly biocompatible.³⁶

1.1.4 Nanomaterials

According to the United States National Nanotechnology Initiative, nanotechnology is the understanding and control of matter at dimensions approximately between 1 and 100 nm that enable unique size-dependent properties. However, there are variations in which nanomaterials in a range of 1 - 1000 nm are considered.³⁷ Nanotechnology also comprises manipulating materials to engineer new structures with special chemical, physical and biological properties at the nanoscale. In this context, nanomedicine has been developed as the branch of science that takes advantage of nanomaterials' properties to diagnose and treat diseases that affect human beings.³⁸ Moreover, the United States National Institute of Health defines nanomedicine as a highly specific medical intervention for the repair of damaged tissues.³⁹ At present, nanotechnology is a multidisciplinary field that has been revolutionizing science since it can be applied to other branches, such as molecular biology, medicine, electronics, robotics, etc. In biomedicine, the use of nanoparticles has led to the design of drug delivery systems, implant coatings, biomarkers, imaging methods, and treatments for diseases, such as cancer, by implementing innovative techniques like hyperthermia to kill cancer cells through the generation of heat.⁴⁰

Classification of Nanostructured Materials

0D Nanostructured Materials (NSMs)

0D nanostructured materials are structures with all dimensions within the nanometric scale (< 100 nm).^{41,42} These nanostructures, considered as point-like particles, include quantum dots, core-shell quantum dots, hollow spheres, nanolenses, etc. One of their main applications is the design of fuel cells that have an efficient catalytic capacity.⁴³ **Figure 1.9** shows in ascending way the classification of these materials according to their dimension.

1D Nanostructured Materials (NSMs)

1D nanomaterials have one dimension greater than 100 nm while the others are at nanoscale.⁴² These nanostructures have an elongated morphological structure such as nanotubes, nanowires, nanorods, nanobelts, etc. Nanostructures of this type are used in nanoelectronics, nanodevices and nanocomposite materials⁴³ (**Figure 1.9**).

2D Nanostructured Materials (NSMs)

2D nanostructured materials are defined as structures with two dimensions on the microscale and one dimension at the nanoscale.⁴² The characteristic nanostructures of this group include branched structures, nanoprisms, nanoplates, nanosheets, etc. This type of nanostructures can have various designs. Thanks to their varied morphology, these structures are used in the design of biosensors, nanocontainers, nanoreactors, etc. At the nanoscale, these materials have properties that differ for those of bulk materials⁴³ (**Figure 1.9**).

3D Nanostructured Materials (NSMs)

3D nanostructured materials are defined with three dimensions at the microscale (> 100 nm).⁴² These nanomaterials can be nanoballs, nanocoils, nanocones, nanoflowers, etc. Their heterogeneous morphology provides these nanostructures with a high surface area offering greater absorption sites for molecules. That is, these 3D nanostructured materials act as transport vehicles for molecules in biological systems⁴³ (**Figure 1.9**).

Synthesis of 0D, 1D, 2D and 3D Nanostructures

Two main methodologies are employed in the synthesis of nanomaterials.

The physical methods are eco-friendly, that is, they do not involve toxic reagents and solvents for the synthesis of nanoparticles.⁴³ The most used for the synthesis of nanostructures are thermal evaporation technique and the sputtering method. In the first case, the evaporated atoms and molecules lose energy when they collide with gas atoms.⁴³ Then, they undergo condensation and are accumulated on a surface of cold powder. In the sputtering method, an argon or helium beam is accelerated towards the surface of a specific material to produce the nanomaterials.⁴³ On the contrary, chemical techniques are more expensive, and some are not eco-friendly. The most used procedure is the template-based, in which a lyotropic liquid crystal template is used to control the size, shape, morphology and porosity of the NSMs.⁴³

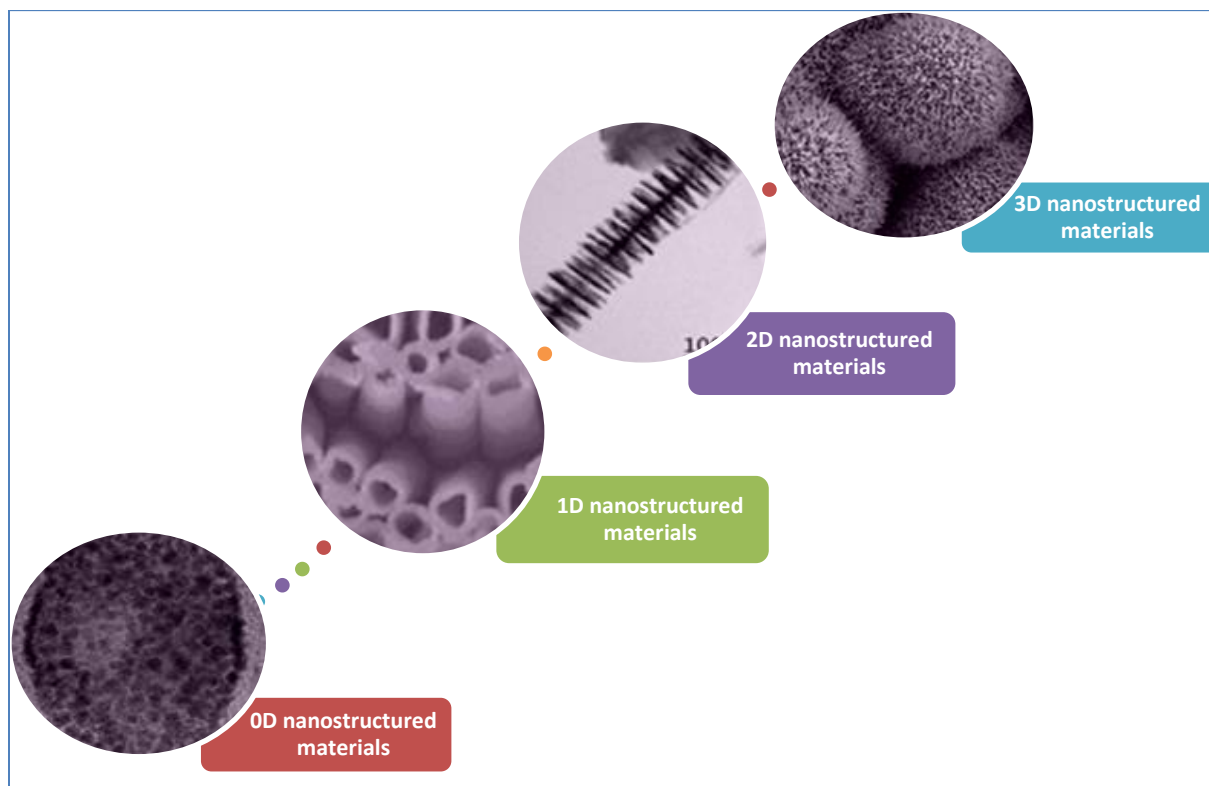


Figure 1.9. Classification of nanostructured materials (0D, 1D, 2D, 3D) with their corresponding shape and size.

Nanomaterials can be classified according to their synthesis methodology:

Synthesis:

Bottom-up

The bottom-up approach starts with simpler molecules or substances. The aim is to build up the particles by taking advantage of the molecules' chemical properties to form chemical bonds. Different processes are used, such as sedimentation and reduction techniques.⁴⁴ The main advantages include better control of the shape and size of the particles.⁴⁴ Some assemblies of molecules can result in two-dimensional structures such as surfaces, ultra-thin films (Langmuir Film), or three-dimensional ones according to their use and functionality.⁴⁵

Top-down

The top-down approach starts from bulk material or large molecules to obtain small particles then transform them into nanoparticles through different processes, such as mechanical milling, chemical etching, chemical vapor deposition (CVD), sputtering and laser ablation.⁴⁴ Top-down methodologies are suitable for large scale production; however, the size and shape of nanoparticles are not entirely controlled.⁴⁴ Lithography is one of the most used methods for the construction of semiconductor transistors.⁴⁵

Particle Replication In Non-Wetting Templates (PRINT)

The PRINT technique (Particle Replication In Non-wetting Templates) is a tool to efficiently create nanoparticles. This process results from the advancement of standard lithography technology to create templates of various shapes, such as spheres, cylinders, discs, etc.⁴⁶ Particles of up to 50 nm can be created precisely with controlled physicochemical characteristics. Besides, the versatility of this technique allows controlling the particle's surface chemistry through post-functionalization or matrix modification processes.⁴⁷ The process consists in creating a perfluoropolyether (PFPE) template from an initial silicon template. Then, in a roll-to-roll

procedure, the particles are placed inside the template to start the drying process employing UV irradiation and evaporation of solvents. Subsequently, the samples of the template are collected on cyanoacrylate and vinyl alcohol films. Finally, once the particles have been collected, the collection layer dissolves while the particles remain in suspension.⁴⁸ **Figure 1.10** illustrates the overall process of PRINT technology.

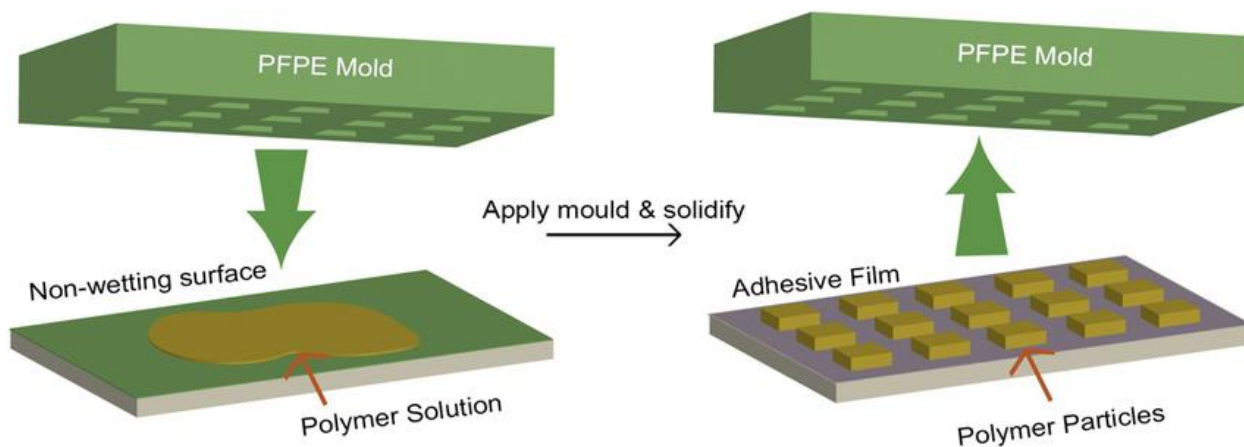


Figure 1.10. Schematic representation of the Particle Replication In Non-wetting Template technology (PRINT) employed to synthesize nanoparticles with a variety of morphologies, sizes and structures. Source: Zhang, et al. (2013). *Advanced materials and processing for drug delivery*.

The main advantages of PRINT technology include a rapid replication of study material for clinical trials and a precise system for mass production of nanoparticles with well-defined morphological characteristics.⁴⁷ Currently, thanks to its versatility, particles of organic and inorganic materials have been synthesized. Print is mainly applied in the pharmaceutical industry to design targeting drug carriers to treat different diseases and avoid unwanted side-effects.⁴⁷

1.1.5 Nanoparticles and Cancer

Drug Delivery Systems

The pharmaceutical industry has invested resources in nanomaterials' research and design to transport and distribute therapeutic agents within the body. The main advantage of using nanoparticles as drug carriers lies in the fact these systems provide greater specificity of the

therapeutic agent in its site of action; that is, they act specifically on the affected tissues, thus avoiding unwanted side-effects and damaging healthy cells.⁴⁹ The materials' physicochemical properties enable the modification of the nanoparticles' external structure to interact directly with the drug or tumor cells.⁴⁹ As a result, this drug-nanoparticle system can reduce the minimum dose, increase bioavailability and reduce the drug's toxicity in the body.⁴⁹ In general, anticancer drugs exhibit low specificity, which is why they affect both healthy cells and cancer or tumor cells. In this context, drug delivery systems are transporting agents that increase the drug concentration in the specific tissue where there are malignant cells (**Figure 1.11**).⁵⁰ Some drug delivery systems are highly versatile as they respond to external stimuli allowing the controlled release of the drug. The most studied nanoparticles in this field are of polymeric and liposomal types. For instance, due to its compatible nature, low toxicity and degradability, chitosan has been screened as a drug delivery system since it can encapsulate some proteins and therapeutic nucleotides; also, it responds to external stimuli like the pH and temperature.⁵⁰ Chitosan NPs can act via passive targeting by taking advantage of the enhanced permeability and retention effect (EPR effect), active targeting through chemical modification of the particles, physical targeting and stimuli sensitive targeting.⁵⁰ The action mechanism of these nanoparticles is based on the functionalization of the nanoparticles' external structure with hyaluronic acid to be captured by tumor cells receptors.⁵⁰ Silica nanoparticles are made of inorganic material and support a large drug load. In that case, drug release is achieved by regulating the size of the nanoparticles; this functional platform can be used as a carrier for gene therapy.⁵¹ Finally, Poly Lactic-co-Glycolic Acid (**PLGA**) is a degradable biomaterial approved by the US Food and Drug Administration for use in the human body; its metabolism produces CO_2 and water. Some PLGA nanoparticles are functionalized with ligands that are recognized by over-expressed receptors on tumor cells.⁵²

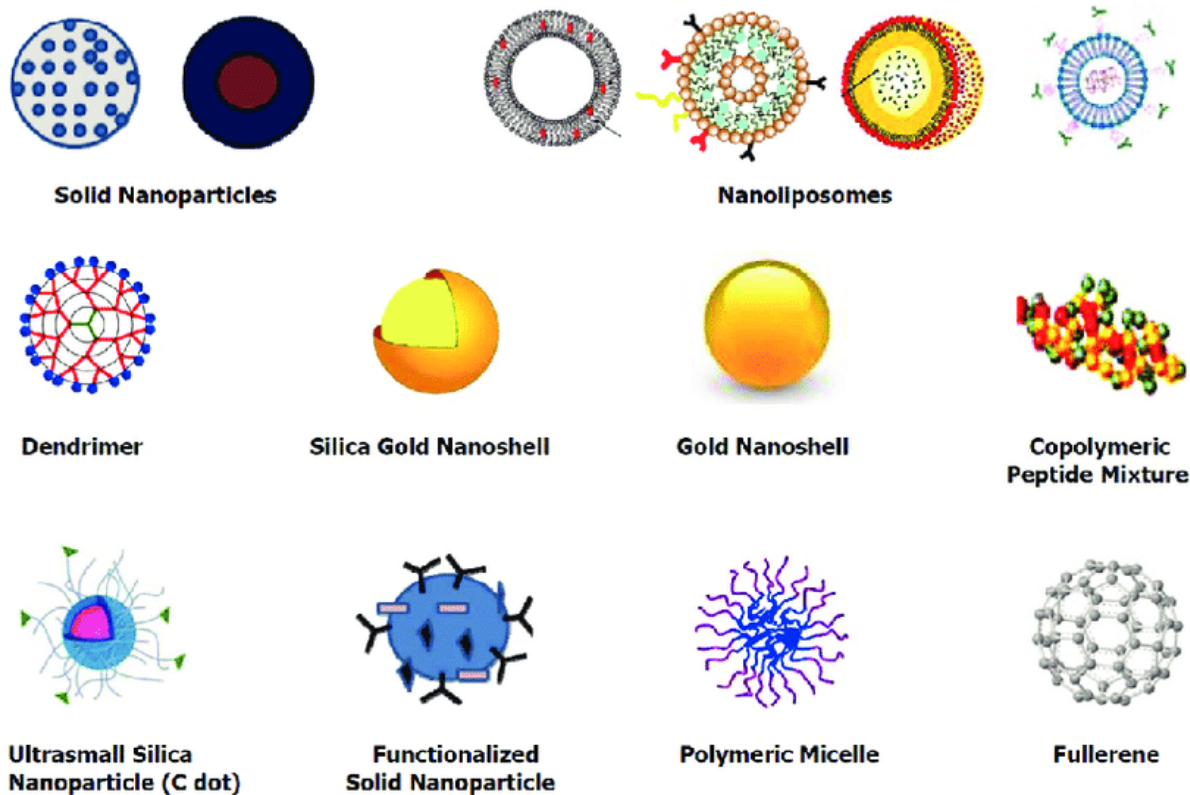


Figure 1.11. Graphical representation of nanoplatforms used as drug delivery systems for cancer treatment and other diseases. These nanoparticles can be organic such as dendrimers, micelles, liposomes, or inorganics, such as quantum dots and gold nanoparticles. Source: Mansour. et al. (2016).

The standard chemotherapy method is unable to distinguish between normal and cancer cells, causing the deterioration of the patient's health and quality of life. For this reason, drug encapsulation has great potential in the field of biomedicine. For instance, the encapsulation of drugs minimizes or suppresses the side-effects since these nanoparticles attach only to damaged tissues. Moreover, it is expected that nanoparticles in the future can work collectively with stem cells to enhance conventional therapy.⁵³

Some tumors have a complex and abnormally functioning vasculature that causes some tumor regions to become hypoxic.⁵⁴ Several studies have focused on inhibiting the expression of the vascular endothelial growth factor and angiogenesis factors to promote a better oxygenation and vascular normalization within the tumor.^{55,56} An abnormal tumor microenvironment contributes to resistance to treatment so that a normal and functional vasculature allows for adequate drug distribution within the tumor.⁵⁴⁻⁵⁶ Additionally, the application of ultrasounds induces an increase

in the tumor's vascular permeability, which improves drug release and absorption. Ultrasound activates nanoparticles so that they can exert their effect through temperature changes.⁵⁷ Di Ianni. et al.(2019), tested a system based on SonoVoe microbubbles, PLGA nanoparticles, and 2 MHz center frequency ultrasound to deliver microRNA as an anticancer therapy in animal models. The outcomes suggested that it may be a viable system for the delivery of therapeutic agents.⁵⁷ The most commonly used polymeric nanoparticles in drug delivery systems are Poly-D,L-Lactide-co-Glycolide Acid (PLGA), Poly Lactic Acid (PLA), Polycaprolactone (PCL), chitosan, and gelatin since they can change their external structure under the effect of certain stimuli. Similarly, micelles can encapsulate the drug to reach its site of action.⁵⁸ Finally, the use of antibodies anchored to the nanoparticle's external surface is a new alternative for detecting proteins present in cancer cells through the use of Surface-Enhanced Raman Spectroscopy (SERS).⁵⁹ The nanoparticle's functionalization with antibodies occurs by forming different chemical bonds, taking into account the antibodies' functional groups to be joined.⁵⁹ Dopamine-mediated bonding, maleimide groups, disulfide bonds, and hydrazide alkyl linker are used.⁵⁹ The use of hollow Au nanoparticles functionalized with antibodies and encapsulated in silica to detect different cancer cells has been reported. The SERS showed the correct detection of the cell line.⁵⁹

1.1.6 Nanoparticles and Bioimaging

Early cancer detection is very important as it enables medical personnel to design effective therapy to attack tumor cells in their early stage of development, and increase around 85% the odds of curing this disease and improve the patient's quality of life.⁶⁰ Fluorescent nanoparticles as diagnostic and treatment entities offer many advantages. For example, they are low-cost systems and provide a high-resolution, real-time imaging for tumors that can be extremely small and are found in deep tissues.⁶¹ To distinguish between cancer cells from normal cells, specific antigens are designed against the receptors of tumor cells. Most cancer cells overexpress the folate receptor that can be targeted using a folic acid ligand.⁶¹ Huang and colleagues, (2016), designed Eu-doped NaGdF₄ NPs coated with polyethylenimine (PEI) and functionalized with folic acid. The in vitro studies showed the potential of these nanoparticles to work as phosphorescent agents.⁶¹ Fu Dongjie. et al. (2020), also developed tripeptide NPs from linear peptides that fluoresce in the green after being excited with ultraviolet light. More specifically, the nanoparticles made with tryptophan residues show a high binding affinity to the cancer drug doxorubicin, yielding a highly

effective drug delivery system against cancer cells.⁶² In vitro bioimaging assays in A549 cells demonstrate that silica nanoparticles engineered from SiCl_4 at the interface of two-phase orthogonal solvents have absorption bands in the UV region (220 - 420 nm).⁶³ Deng et al constructed Mn^{2+} doped $\text{NaLuF}_4:\text{Yb}/\text{Er}$ NPs following the lanthanide-doped upconversion method and verified that these nanoparticles could emit red fluorescent light in 650 - 670 nm region for applications as a contrast agent in magnetic resonance image of deep tissues.⁶⁴

X-ray Bioimaging

The use of nanoparticles that act as carriers of contrast agents has become a topic of great relevance in medicine since they can help to detect cancer early, determine the anatomical position of cancerous tissue and image-guided surgery.⁶⁵ Contrast agents are substances in aqueous solution that better absorb X-rays. These contrast agents are extensively used in the clinical field to differentiate healthy tissues from adjacent tumor tissues. The most commonly used substances have an aromatic ring as their central component and halogen atoms linked to their chemical structure, as shown in **figure 1.12**.⁶⁶

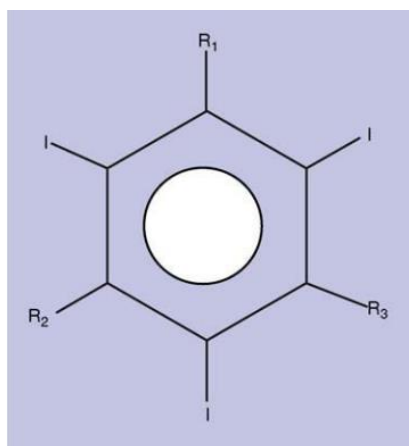


Figure 1.12. Chemical structure of contrast agents employed to improve X-ray bioimaging. Source: Speck, U. (2008)

These substances are biocompatible, non-toxic and do not link to biological receptors within the human body. However, there are still some limitations, such as high viscosity and ionic charge, that make them interact with tissues causing toxicity.⁶⁷ In this sense, the development of

nanoparticulate contrast agents is a novel alternative that seeks to enhance conventional contrast agents. Much research seeks to improve the solubility, viscosity and osmolality of these contrast agents and achieve safer biological performance to avoid nephropathies, cardiac events, and renal toxicity.⁶⁷ An example of this is the design of colloidal nanosuspensions containing iodine atoms targeting macrophages. They are approximately 250 nm in size, and their main purpose is to detect atherosclerotic plaque.⁶⁷ Similarly, the use of gold nanoparticles as contrast agents for X-ray computed tomography has been investigated.⁶⁸ Another study proved that PTFE felt pledgets used as a support material to reinforce cardiovascular tissue sutures show high attenuation to the X-rays produced in a multislice computed tomography (MSCT) analysis in patients with prosthetic heart valves.⁶⁹ **Figure 1.13** displays the attenuation of PTFE felt pledgets under X-rays inside the body.

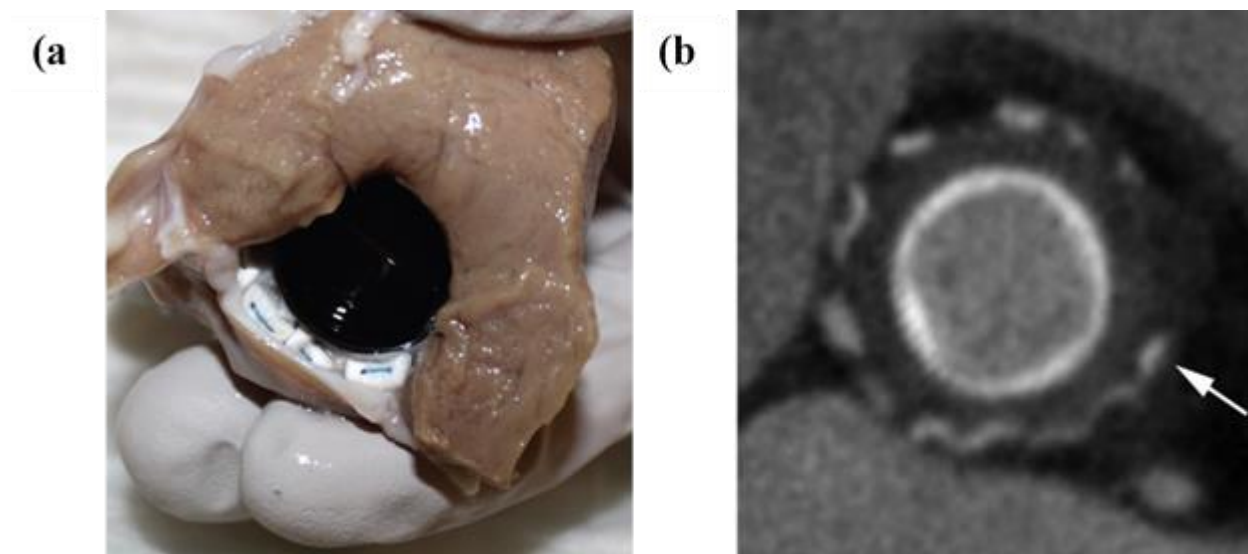


Figure 1.13. PTFE felt pledgets. **(a)** PTFE felt pledgets inserted into the cardiovascular tissue to reinforce sutures. **(b)** X-ray attenuation of PTFE felt pledgets. The image shows that PTFE previously inserted are clearly visible under X-rays. This allows the identification of abnormalities in the felt pledgets non-invasively. Source: Habets. et al. (2012).

Finally, another promising alternative is the application of iodinated polyvinyl alcohol (PVA) polymeric nanoparticles. The results showed great effectiveness as contrast agents in the

cardiovascular system, liver and spleen in spectral photon counting computed tomography, as evident in **figure 1.14**.⁷⁰

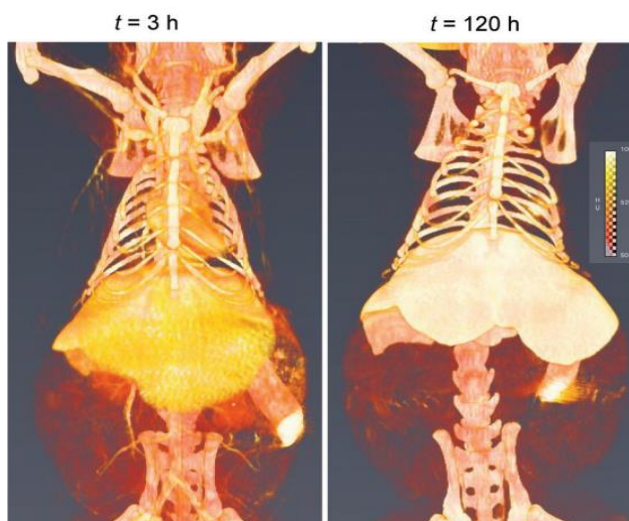


Figure 1.14. Computed tomography image after 3h and 120h of intravenous injection of iodinated polyvinyl alcohol nanoparticles to enhance the imaging of the abdominal region. Source: Balegamire (2020).

Table 1.3 compiles the main advantages, disadvantages and applications of X-ray bioimaging.

Table 1.3. Advantages and disadvantages of the application of X-rays in the clinical practice. Source: Medical X-ray Imaging | FDA

| Advantages | Disadvantages |
|--|--|
| <ul style="list-style-type: none"> - Noninvasively and painlessly help to diagnose disease and monitor therapy. - Support medical and surgical treatment planning. - Guide medical personnel as they insert catheters, stents, or other devices inside the body. - Treat tumors. | <ul style="list-style-type: none"> - X-ray imaging uses ionizing radiation to generate images of the body. - Tissue effects such as cataracts, skin reddening, and hair loss, which occur at relatively high levels of radiation exposure. - Ionizing radiation has enough energy to potentially cause damage to DNA. |

- Remove blood clots or other blockages.

Ultrasound Bioimaging

Contrast agents are substances that can be administered by bolus or infusion into the bloodstream or cavities and have specific physicochemical and biological properties that improve the signals acquired by ultrasound. An ideal contrast agent should be biocompatible, intravenously injectable and have high tissue specificity. Commercial contrast agents for ultrasound systems are made up of microcapsules that enclose an inert gas, generally perfluorocarbon, air, and sulfur hexafluoride⁷¹

Figure 1.15 illustrates an example of nanobubble utilized in ultrasound bioimaging.

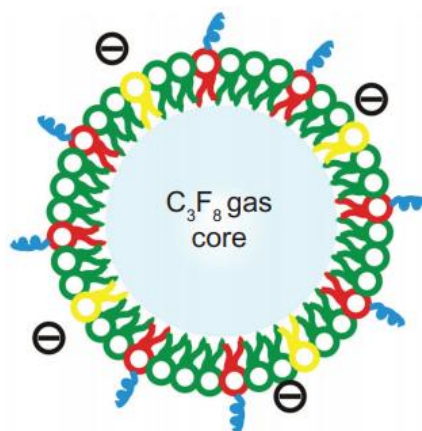


Figure 1.15. Nanobubble composed of a polymeric shell enclosing the core composed of C_3F_8 gas. Source: Zheng, et al (2012).

The physicochemical properties of the shell determine the stability and durability of the bubbles, while the inert gas defines the acoustic properties. The composition of the shell varies from phospholipids to capsules based on proteins, such as albumin.⁷² Depending on the shell's properties, such as size, composition and surface characteristics, different organs can be targeted.⁷³ For example, perfluorocarbon bubbles ranging from 1-10 μm can circulate through the systemic

circulation entering the pulmonary vascular system.^{72,73} In this sense, polymeric nanoparticles serve as good ultrasound contrast agents (UCAs) thanks to their mechanical properties and high biocompatibility. The versatility of these systems enables the remodeling of their surface composition easily and even the loading of hydrophobic and hydrophilic species to improve the obtained images. However, the design of nanoparticles remains a challenge because the image acquired by ultrasound is of low resolution and has numerous noise sources that make the study of the internal structures difficult.⁷⁴

To overcome this obstacle, an *in vivo* study carried out on New Zealand rabbits confirmed the effectiveness of polylactic acid (PLA) nanoparticles loaded with gold nanorods as a good contrast agent to explore the kidney vasculature employing ultrasound imaging.⁷⁵ **Figure 1.16** illustrates the effectiveness of this technology by using nanoparticles as contrast agent. **Table 1.4.** summarizes the main advantages and disadvantages of ultrasound imaging.

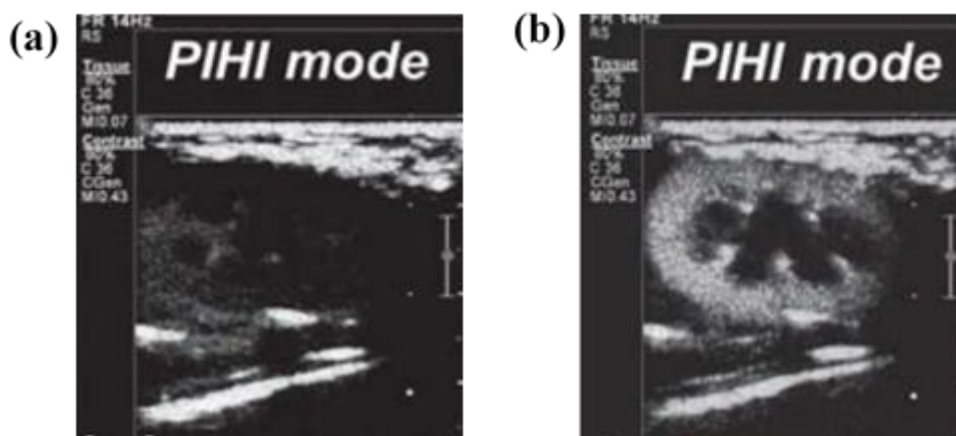


Figure 1.16 Ultrasound contrast agent composed of a lipid shell (PLA) loaded with gold nanorods to image the kidney vasculature. Source: Ke. et al. (2011).

Table 1.4. Advantages and disadvantages of ultrasound as an imaging system. This system has multiple advantages compared to x-ray technology. Source: Shung, (2005).

| Advantages | Disadvantages |
|--|---|
| - Ultrasound is a form of nonionizing radiation and is considered safe to the best of present knowledge. | - Organs containing gases and bony structures cannot be adequately imaged without introducing specialized procedures. |

-
- | | |
|---|---|
| <ul style="list-style-type: none">- It is less expensive than imaging modalities of similar capabilities.- It produces images in real time, unattainable at the present time by any other methods- It has a resolution in the millimeter range for the frequencies being clinically used today, which may be improved if the frequency is increased.- It can yield blood flow information by applying the Doppler principle- It is portable and thus can be easily transported to the bedside of a patient. | <ul style="list-style-type: none">- Only a limited window is available for ultrasonic examination of certain organs, such as the heart and neonatal brain.- It depends on operator skill.- It is sometimes impossible to obtain good images from certain types of patients, including obese patients. |
|---|---|
-

1.2 Problem Statement

According to the WHO, there were worldwide 18 million cases in 2018 of cancer and around 9.6 million deaths.²¹ By 2040, it is estimated to be 27 million new cancer cases every year and up to 16 million deaths from this disease. The most common cancer risk-factors are the lack of physical activity, non-adequate diet, alcohol consumption and smoking. Cancer also represents about 1.16 trillion \$ of expenditure per year worldwide.⁷⁶ A critical factor in improving these statistics is the lack of tools that allow the early diagnosis to design an efficient treatment to avoid cancer development and symptoms. Hence, it can be said that early detection and treatment are critical to prevent cancer development and metastasis to other organs, resulting in less morbidity and lower costs globally. On the contrary, when cancer is detected in the late stages, many organs are affected, and the treatment becomes ineffective and expensive. According to the WHO, in Latin America and the Caribbean, approximately 1.2 million new cancer cases each year are reported causing the death of around 600,000 people.⁷⁷ Thus, globally, public campaigns promote better control of the leading causes to decrease the mortality rate. The aim is to implement the European code against cancer, which consists in recommendations to reduce cancer risk factors. Till 2030, the WHO estimates a 65% increase in the appearance of new cancer cases and 75% of mortality if the main risk factors are not mitigated.⁷⁷

According to the Global Cancer Observatory (GLOBOCAN), cancer has an incidence of 157.2 cases per 100,000 inhabitants in Ecuador, 2020.²³ In this sense, using technologies such as ultrasound imaging, radiography and X-ray computed tomography combined with nanotechnology is an innovative alternative focused on enhancing conventional diagnostic systems by providing better contrast of the affected tissues. In clinical practice, these imaging methods are the first line of diagnosis that enable the early detection of cancer. However, it is essential to emphasize that, beyond current treatments, such as chemotherapy and radiotherapy, Ecuador does not have an ongoing investigation that favors the development of new treatments and diagnosis opportunities for cancer patients. In this sense, nanotechnology research that opens new opportunities to develop better diagnostic and treatment methods is an essential and necessary step. The use of nanomaterials to diagnose and treat cancer is one of the most promising biomedical approaches since these can act as carriers of drugs, bioimaging agents, tumor markers, and even, therapeutic agents by themselves. For this reason, it is crucial to exploit the properties of nanoparticles as a

potential, versatile and cost-effective alternative for cancer imaging and treatment in affected patients in low-income countries.

1.3 General and Specific Objectives

General objective:

This thesis aims at synthesizing and analyzing pure PTFE nanoparticles using spectroscopic and characterization techniques and their implementation as an alternative for the diagnosis and treatment of cancer through bioimaging systems such as X-rays and ultrasound.

Specific Objectives:

- Synthesize pure PTFE nanoparticles starting from cheap commercially available products.
- Characterize the produced PTFE nanoparticles to assess their physical, chemical, and morphological characteristics.
- Obtain chemically pure PTFE nanoparticles.
- Analyze the attenuation of X-ray and ultrasound irradiation by the pure PTFE nanoparticles.
- Analyze the data obtained during the biomaterial characterization applying the knowledge acquired during the professional training process.
- Present the advantages of using nanoparticles as an alternative for the diagnosis and treatment of cancer.
- Present the properties of PTFE as a versatile material and its applications in other fields of biomedicine.

CHAPTER 2

METHODOLOGY

This chapter presents the theoretical basis used to carry out this project. All the information presented here is obtained from scientific articles and books that allow the understanding of the techniques implemented to synthesize and characterize the PTFE nanoparticles. The development of this project is divided into two sections to facilitate the reader's comprehension.

- **Synthesis of fine PTFE powder and nanoparticles:** This section details the protocol applied for the synthesis and the collection of pure PTFE nanoparticles. In the same way, the synthesis contains two essential parts. The first part describes the synthesis of PTFE fine-powder while the second part describes the downsizing of this powder to obtain the nanoparticles.
- **Characterization:** This part details the techniques employed to characterize the PTFE fine powder and nanoparticle samples to obtain a complete view of the properties of the studied material.

2.1 Synthesis of PTFE Fine-powder.

The PTFE fine-powder was synthesized using "WEICONLOCK AN 301-65 Pipe and Flange ® sealing". The protocol applied is based on a modified version of the previous work elaborated by Cristhian Chingo during his thesis project.

Materials.

1. WEICONLOCK AN 301-65 Pipe and Flange sealing by JEV Soluciones en Ingeniería (Quito - Ecuador).
2. Acetone 180 ml.
3. Ethanol 70 %.

Methodology

First, 6 g of WEICONLOCK sealant and 30 mL of acetone are added into a 50 mL Falcon tube. This process is carried out inside a fume hood owing to acetone volatility. Next, the tube is sealed with parafilm to avoid leaking and vortexed at 200 rpm for 10 min. Finally, the tube is placed in the shaker for 24 h at room temperature (RT). After that, a white suspension is formed that is, subsequently, centrifuged using Thermo Scientific Sorvall Legend XTR™ Centrifuge at 4000 rpm for 15 min. At this point, the phase separation occurs: a yellow supernatant and a white pellet are formed. Using a pipette, the supernatant is discarded whereas the white pellet is kept to undergo several washing cycles till all the additives and organic compounds are totally removed. Typically, a given volume of alcohol 70% is added to the tube that contains the pellet to give rise to a yellowish suspension; then, the tube is vortexed at 200 rpm for 10 min. After that, the same tube is centrifuged at 4700 rpm for 15 min to trigger a phase separation: sedimented PTFE particles and a supernatant. This process is repeated till the supernatant becomes transparent. Once the samples are clean, 30 mL of HF (37%) are mixed with the white PTFE powder in a Falcon tube, then placed in the Vortexer at 200 rpm for 10 min and finally into the shaker for 48 h. Finally, the samples are washed three times using the same process described above using alcohol 70% and dried in the oven at 60 °C for 48 h. **Figure 2.1** shows the overall process of PTFE fine-powder synthesis.

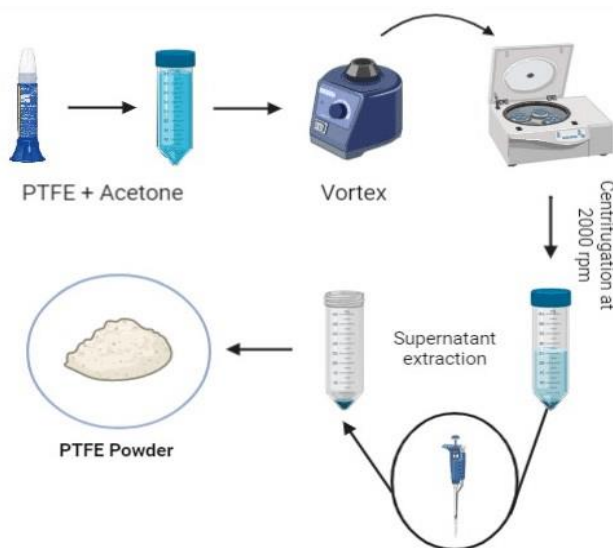


Figure 2.1. Graphic description of the PTFE fine-powder synthesis process.

2.2 Production of PTFE Nanoparticles

Once the fine PTFE powder is synthesized, the next step is the production of the nanoparticles. This process is carried out by dispersing the fine powder in ethanol to obtain a homogeneous population of PTFE nanoparticles.

Materials

1. Ethanol absolute CAS 64-17-5 for analysis EMSURE® ACS,ISO,Reag. Ph Eur.
2. TWEEN® 80
3. PTFE fine-powder (previously produced)

Methodology

In a falcon tube of 15 mL are added 10 mL of ethanol and 0.12 g of PTFE powder. The tube is then sealed and hand shaken vigorously. After that, the tube was immediately placed into an ultrasonic cleaner Branson 1510 DTH for 1 h at 22 °C. Then, the supernatant is extracted while the sedimented material is left in the tube. The supernatant is placed in a 50-mL baker to which 1% (v/v) of TWEEN® 80 is added for subsequent sonication. The sonication is made with a Cole-Parmer® Ultrasonic Processor at an amplitude of 72% for 30 min. This system of sonication is made with a probe introduced directly into the solution. After that, the solution is placed back in a falcon tube of 15 mL to perform the differential centrifugation using a Hettich ZENTRIFUGEN EBA20 at 6000 rpm for 30 min. Finally, an aliquot of the supernatant, which is almost transparent because it contains the PTFE nanoparticles, is sent to characterization.

2.2.1 Sonication

Ultrasound has several applications in medicine, from an imaging tool to the synthesis of nanoparticles. In bioengineering, ultrasound is used to break up large particles into smaller nanoparticles. Depending on the nanoparticle's characteristics, the sonication process influences the behavior of the nanoparticles. In this sense, ultrasound can disperse (dissolve) or agglomerate

nanoparticles and interact or not with the molecules or compounds in their vicinity. The general protocol prescribes a certain amount of acoustic energy to ensure that the agglomerates dissociate and achieve the appropriate size of the nanoparticles.⁷⁸ The working principle of this technique demonstrates that, in organic molecules, the shock wave created by ultrasound interacts with the particles, resulting in their breakdown into smaller particles. Commonly used frequencies are located between 20 kHz to approximately 480 kHz and power of ~10 W. It is known that the lower the frequency, the faster size reduction of the nanoparticles. At lower frequencies, stronger shockwaves are generated as a result of the production of large cavitation bubbles. In the same way, high power levels result in a decrease in the size of the particles. However, there is no evidence of the influence of power levels on high or low frequencies. **Figure 2.2** shows that particles can be broken by fracture or by abrasion. In the first case, the particle fragments into smaller particles while small particles are detached from the edges of the massive particle in the second case.⁷⁹ Thus, increasing the intensity of sonication and the surfactant concentration leads to the production of smaller nanoparticles.⁸⁰ The sonication technique is also used to break up agglomerated powder suspensions owing to their interaction with cavitation bubbles formed in the liquid.⁸¹

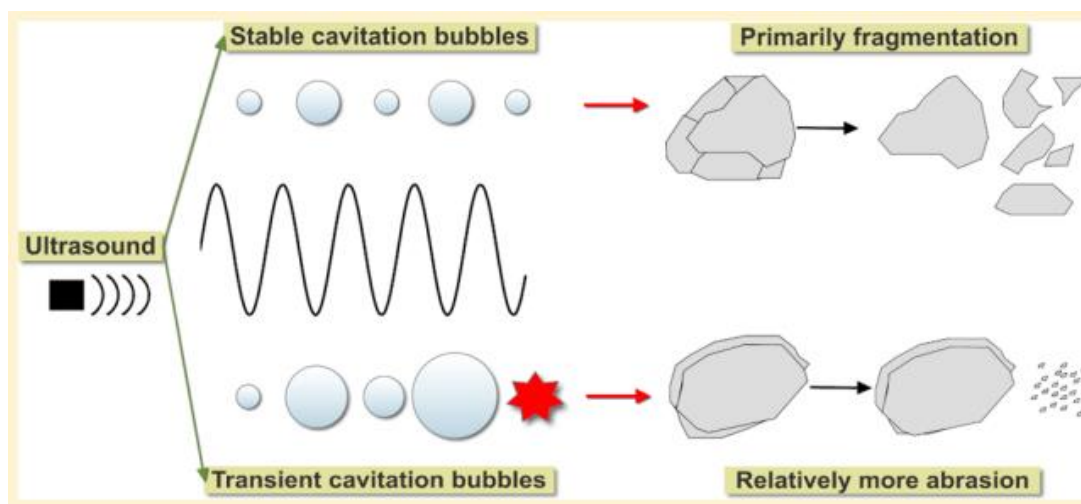


Figure 2.2. Ultrasonic fragmentation process of agglomerate particles. Depending on the stability of cavitation bubbles, it is possible to identify two types of particle fractioning. Particle fragmentation occurs in the presence of stable cavitation bubbles. On the other hand, particle abrasion occurs when transient cavitation bubbles are formed. Source: Jordens. et.al. (2016).

2.3 Characterization Techniques

2.3.1 X-ray Diffraction

X-ray diffraction is a non-destructive technique that enables the determination of the crystalline structure, lattice parameters, crystalline sizes and chemical composition of a material. As can be seen in **Figure 2.3**, the X-ray generation takes place in a vacuum chamber. The cathode is made up of a tungsten filament that emits electrons that are subsequently accelerated with a voltage of 40 kV towards a rotating copper or molybdenum anode. 90% of the accelerated electrons dissipate as heat and 10% generate X-rays that allow crystallographic analyses.⁸² Bragg's law relates the scattering of X-rays to the crystalline structure of a material through the following equation:⁸³

$$n \lambda = 2 d \sin(\theta) \quad (2.1)$$

Where:

- θ = scattering angle
- d = interplanar distance
- n = order of the diffraction peak
- λ = wavelength of the X-ray

In XRD, X-rays interact with the electrons that form the crystalline structure of a material or powder. In this sense, the scattered X-ray photons provide information on how electrons are distributed in the nanoparticles' structure. The result is a diffraction pattern that indicates the distribution of the atoms in the studied material.⁸⁴

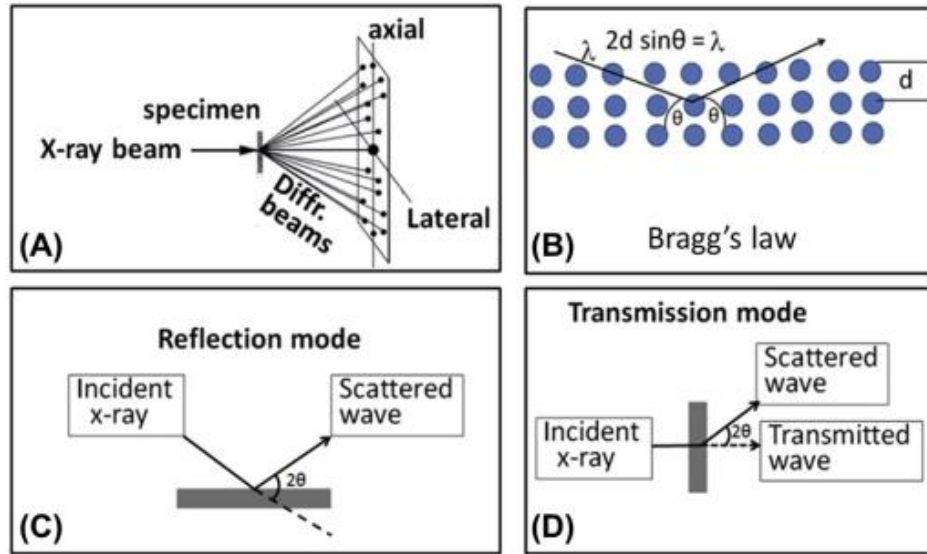


Figure 2.3. Working principle of X-ray diffraction. (A) X-rays interact with the sample. Subsequently, the scattered X-rays are collected by a sensor to generate a diffraction pattern. (B) Bragg's law allows the investigation of the arrangement of the crystalline planes with their respective spacing distance. (C) Data collection based on reflection X-ray diffraction in which X-rays do not entirely penetrate the sample. (D) Data collection based on the transmission of X-ray diffraction. X-rays pass through the sample and a sensor collects scattered X-rays. Source: Singh. et al. (2016).

Specifically, X-ray diffraction allows the determination of:

1. The orientation and crystal structure of a known or unknown sample
2. The size and orientation of the crystalline regions
3. Atomic arrangement in crystals
4. Crystallite size
5. Structural parameters, such as lattice parameters and crystallite size
6. Index of crystallinity

The crystallite size is deduced from the Scherrer equation⁸⁴:

$$D = \frac{k\lambda}{\beta \cos \theta} \quad (2.2)$$

Where.:

1. **D**: diameter in nm
2. **κ** : particle symmetry
3. **λ** : X-ray wavelength
4. **θ** : Bragg's angle at which the peak is observed
5. **β** : full width of diffraction line at half maximum intensity

2.3.2 Scanning Electron Microscopy

Scanning Electron Microscopy (SEM) is a technique used to study the microstructure of materials generating a three-dimensional topographic image of the structure and provides information about the morphology and composition of the surface. The device comprises an electron source, electromagnetic lenses to focus the electrons, an electron detector, sample cameras, computers and screens to display the images. The procedure consists in accelerating electrons through the lenses to create a fine beam of electrons. This fine beam of electrons strikes and penetrates the sample to a depth of a few microns. The signals generated from this interaction, such as electrons and photons in the form of X-rays, are interpreted by the scattered energy X-ray spectrophotometer detector that generates the structure of the studied sample.^{84,85} This technique is schematically shown in **Figure 2.4**. This technique allows observing the surface of a material with up to 35,000 times of magnification. The results depict the topology, size, shape, crystalline organization and the electrical conductivity of the material.^{86,87} The main advantages of SEM reside in its ability to examine a large number of samples of different natures (metals, alloys, polymers, rocks, nanodevices, powders, nanoparticles, etc.) and form three-dimensional images. Moreover, it is fast, easy to implement and non-destructive with a spatial resolution of 1 nm.⁸⁵

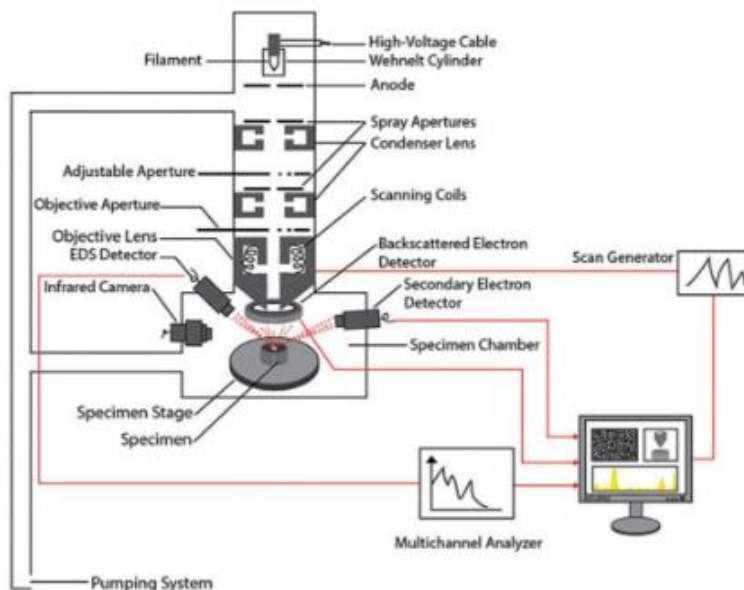


Figure 2.4 Schematic description of the image formation process and chamber components of Scanning Electron Microscopy. Source: Anwar. et al. (2018)

2.3.3 Transmission Electron Microscopy

Transmission Electron Microscopy is a high-resolution technique that identifies the size, shape, and crystallinity of nanostructures with a resolution of up to 0,1 nm. Generally, the process consists in focusing an electron beam through two condenser lenses that filter the high-angle beams and let only low-angle electrons pass to the sample.⁸⁸ In this system, the electron beam passes through the sample at an acceleration of 80-200. The passing electrons are scattered due to the internal structure or crystalline phase of the material. The X-rays produced are detected and form the image.⁸⁶ The whole process is shown in **Figure 2.5**.

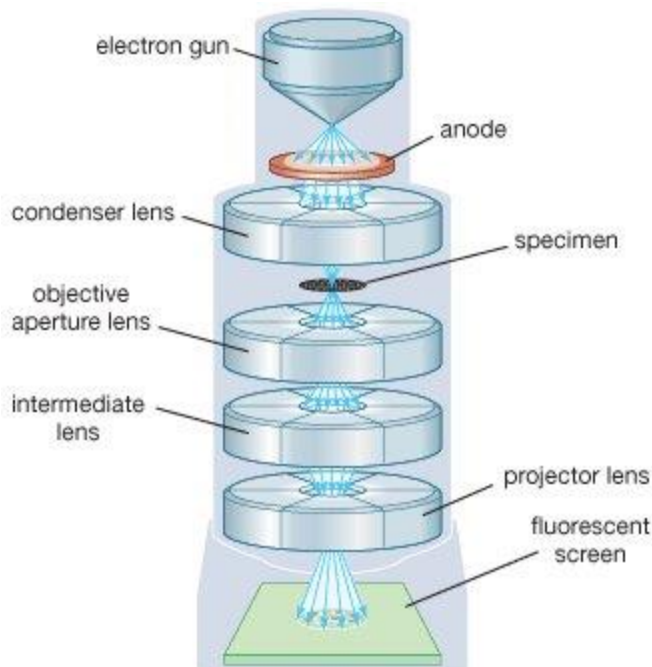


Figure 2.5. Transmission Electron Microscopy system for image obtainment. The electron gun passes through the sample and the scattered electrons are detected to form the image. Source: Transmission electron microscope | instrument | Britannica.

2.3.4 UV–Vis analysis

The ultraviolet-visible spectroscopy measures the absorption of light by a material as a function of the incident wavelength. The analysis region can be determined by defining the wavelengths of interest. For visible light, the corresponding wavelength is 380-740 nm. The ultraviolet region is below 380 nm while the infrared corresponds to wavelengths greater than 740 nm. Each substance has different states of electronic energy, which makes the absorbed radiation different for each sample. Additionally, because energy is inversely proportional to wavelength when the nanoparticle size increases, lower energy radiation is absorbed. The spectrum obtained provides information on the electronic properties of the sample.⁸⁴ For a molecule to absorb light, the light's energy must match a specific, quantized energy gap. For this reason, each molecule has its own absorption spectrum due to its electronic arrangement. Therefore, the light of a particular wavelength will excite an electron from the ground state to a high energy state.⁸⁹ Specifically, spectroscopy is defined as absorption and reflectance in the UV-Vis spectral region. Light energy absorption occurs as the molecules contain π electrons or n electrons that absorb energy from UV-

Vis light and are excited towards anti-bonding molecular orbitals. The Lambert-Beer law governs this spectroscopic technique:

$$A = \text{Log}_{10} \left(\frac{I_0}{I} \right) = \epsilon CL \quad (2.3)$$

Where:

- A: absorbance
- I_0 : incident intensity
- I: transmitted intensity
- L: light path length through the sample
- C: concentration of absorbing species
- ϵ : molar absorptivity

Prior to recording the sample spectra, a calibration of the equipment is necessary. In the case of solid samples, the measurement is made only on the surface.⁹⁰

2.3.5. X-ray Photoelectron Spectroscopy (XPS)

XPS is a quantitative elemental analysis technique that involves the detection of photoelectrons emitted as a result of interaction of the atoms of the sample with X-rays to investigate the surface composition. X-rays penetrate the sample up to 7-10 nm in depth. Photoelectrons close to the surface that escape without loss of energy appear as peaks as a function of binding energy. The binding energy is determined from the average kinetic energy of the emitted photoelectrons. The working principle of this mechanism is presented in **Figure 2.6**. The energy of the photoelectrons is characteristic of each element; therefore, it allows to identify all the chemical elements that make up a sample, except for hydrogen and helium.^{91,92} XPS data is collected in two ways. The first consists in a wide survey spectrum in which data is collected in a range of 1000 eV to quantify the actual composition of the sample. On the contrary, in high-resolution scans, narrow energy windows are defined to determine the specific chemical state of the elements.⁹³

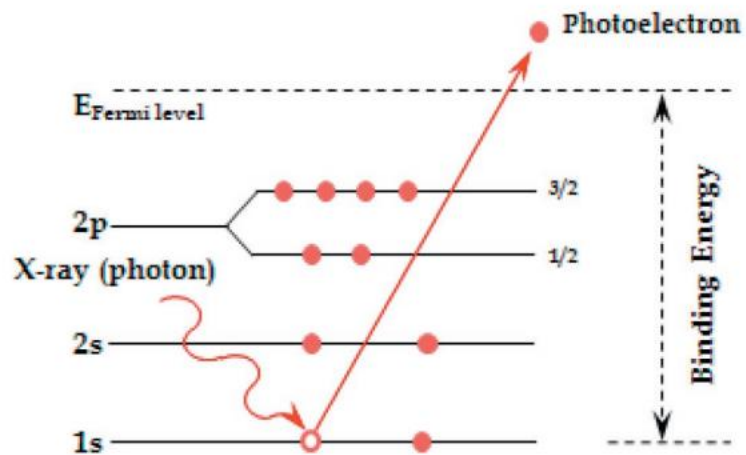


Figure 2.6. Diagram of the photoelectric effect that governs the XPS technique. The X-rays penetrate the sample and the emitted photoelectrons are detected to identify the elements that constitute the material. Source: Engelhard, et al. (2017).

CHAPTER 3

RESULTS & DISCUSSION

This chapter details the equipment, materials and protocols employed during the implementation of the present thesis project.

3.1 Characterization

3.1.1 Diffuse Reflectance UV-Vis Analysis (PTFE Fine-powder)

UV-Vis diffuse reflectance is a technique that allows knowing the electronic properties of PTFE when it absorbs light. The device used for this analysis was a LAMBDA 1050 UV / Vis PerkinElmer® spectrophotometer that includes the accessory PerkinElmer® 3D WB detector module. To analyze the PTFE fine-powder, the Praying Mantis™ Diffuse Reflection Accessory is used. This accessory contains a sample holder with a 3-mm diameter and 3-mm deep hole into which the fine PTFE powder is introduced. The reflectance was recorded between 200–800 nm. Before taking the measurement, the device was calibrated with a BaSO₄ white standard as a blank standard. The pattern obtained in the UV-Vis spectroscopy of PTFE fine-powder is shown in **Figure 3.1a**.

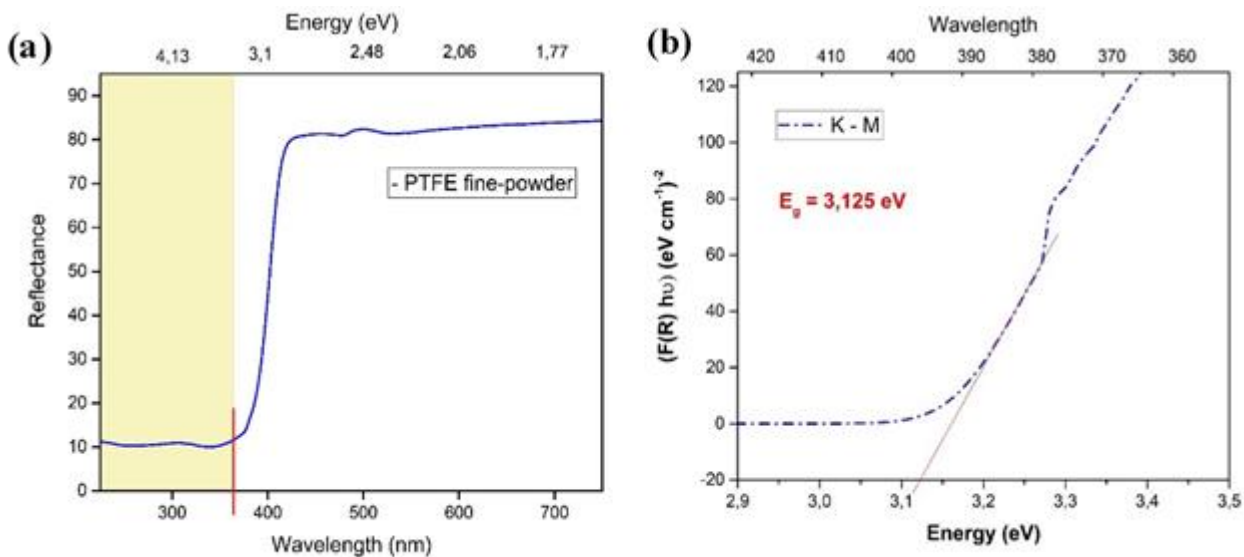


Figure 3.1. (a) Diffuse reflectance spectroscopy spectra of PTFE fine powder in the range of 200–800 nm. (b) Kubelka-Munk transformation to estimate the band gap of the same material.

Kubelka–Munk Transformation

The Kubelka-Munk transformation is applied to analyze the reflectance spectrum and estimate the energy band gap of PTFE. The Kubelka - Munk (K-M) function is defined as follows⁹⁴:

$$F(R) = \frac{k}{s} = \frac{(1 - R)^2}{R} \quad (3.1)$$

Where:

- k = absorption coefficient
- s = scattering coefficient
- R = reflectance

However, to apply the Kubelka-Munk function, it is necessary to transform the data from wavelength to energy using the Einstein-Planck relationship:

$$E = h\nu = \frac{hc}{\lambda} \quad (3.2)$$

Where:

- h = Planck constant
- ν = frequency
- λ = wavelength
- c = speed of light (2.99×10^{17} nm s⁻¹)

For example, randomly taking a wavelength value ($\lambda = 400$ nm) from the reflectance spectrum is necessary to perform the subsequent calculations:

$$E = h\nu = \frac{hc}{\lambda}$$

$$E = h\nu = \frac{4.135667 \times 10^{-15} * 2.9979 \times 10^{17}}{400}$$

$$E = h\nu = 3.125 \text{ eV}$$

Subsequently, to calculate the reflectance value, it is necessary to divide by 100 the reflectance value obtained in the spectrum, associated with its respective wavelength.

$$R = \frac{\%R}{100} \quad (3.3)$$

$$R = \frac{44.21}{100} = 0.4421$$

The molar absorption coefficient (K) is determined from the reflectance value obtained in the previous step, applying the following equation:

$$K = (1 - R)^2 \quad (3.4)$$

$$K = (1 - 0.4421)^2 = 0.3112$$

Then, to calculate the scattering coefficient, it is necessary to use the next equation:

$$S = 2R \quad (3.4)$$

$$S = 2 * 0.4421 = 0.8842$$

Likewise, the Kubelka-Munk function, F(R), can be interpreted in terms of the molar absorption coefficient and the scattering factor, therefore:

$$F(R) = \frac{k}{s} \quad (3.5)$$

$$F(R) = \frac{0.31125}{0.8842} = 0.35202$$

Finally, to estimate the bandgap energy of PTFE, it is necessary to calculate the factor $[(\frac{k}{s})hv]^2$, therefore:

$$[0.35202 * 3.1]^2 = 1.19082$$

This process is repeated for each of the reflectance spectrum wavelength values (200-800 nm). **Figure 3.1b** shows the Kubelka-Munk transformation applied to the data obtained from the reflectance pattern (**Figure 3.1a**). The factor $[(k/s)hv]^2$ is located on the Y-axis, while the energy values are established on the X-axis. The bandgap of PTFE is equal to approximately 3.125 eV.

The reflectance spectrum determined that PTFE absorbs about 90% of the electromagnetic energy of incident light, in the ultraviolet region up to about 300 nm. Starting from ~400 nm the reflectance value increases exponentially to approximately 80% (**Figure 3.1a**). In this sense, the reflectance spectrum shows a large percentage of electromagnetic radiation absorption for wavelengths within the ultraviolet region, which means no reflectance. Additionally, **Figure 3.1b** displays the pattern obtained after applying the K-M transformation in which the band gap is determined to be 3.125 eV. The energy gap value suggests that this sample acts as an insulator material. Therefore, light with an energy greater than 3.125 eV can excite the valence electrons to the conduction band.

3.1.2 X-ray Diffraction (PTFE Powder)

X-ray diffraction (XRD) analysis was carried out using a PANalytical brand θ - 2θ configuration (generator-detector) X-ray tube with copper $K\alpha$ irradiation ($\lambda = 1.54059 \text{ \AA}$) and EMPYREAN diffractometer. The obtained XRD pattern of the sample displays solely the characteristic peaks of PTFE as depicted in **Figure 3.2**; this strongly suggests that the obtained sample is pure as no contamination is seen.

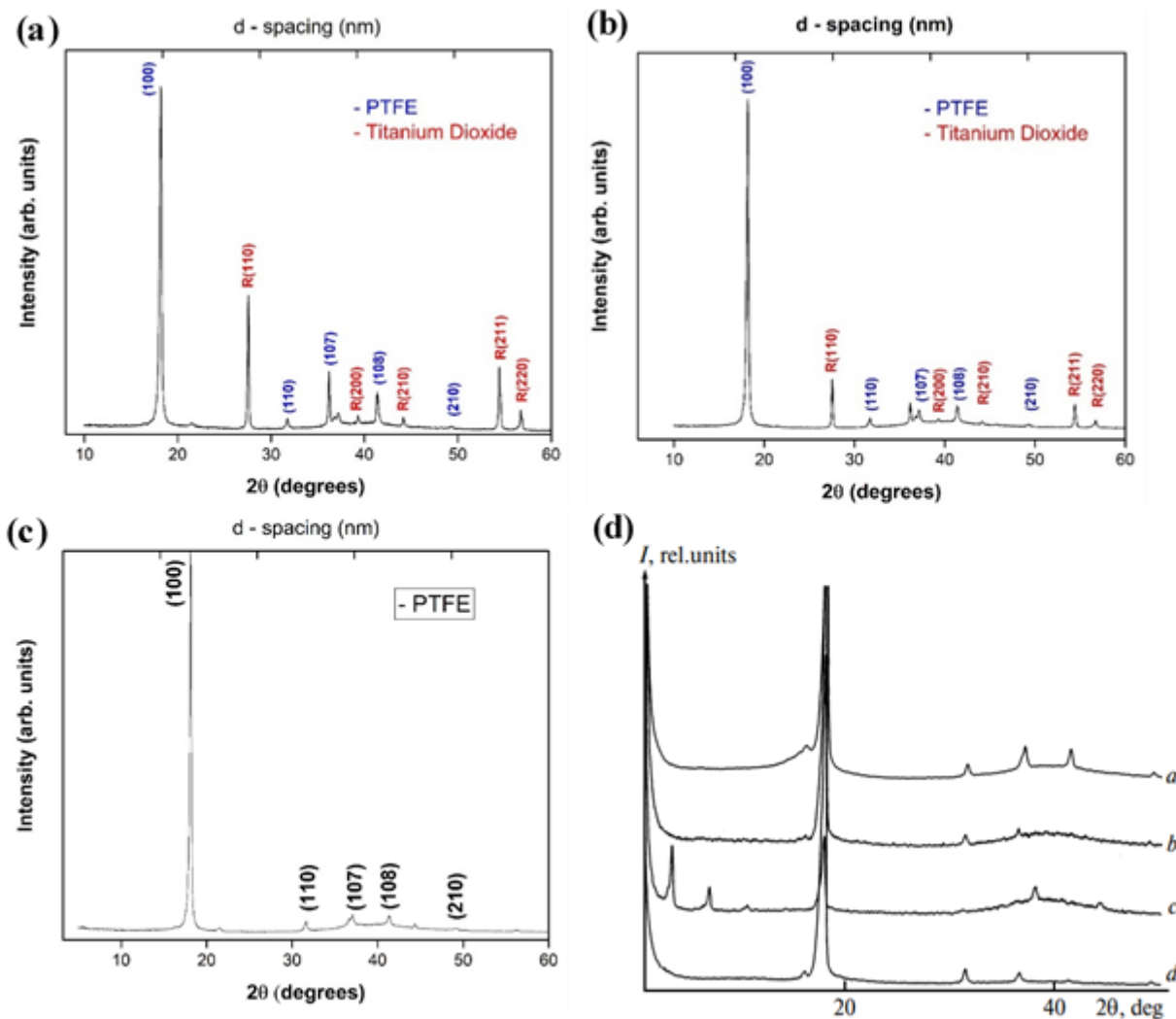


Figure 3.2. Diffraction patterns of PTFE. (a) The diffraction pattern of PTFE synthesized only with acetone without contact with hydrofluoric acid reveals intense peaks characteristic of titania as an inorganic contaminant. (b) Diffraction pattern obtained after exposing the sample to hydrofluoric acid for 24h. The peaks corresponding to titania have a lower intensity, which indicates a reduction of the contaminant. (c) The diffraction pattern recorded after PTFE exposure for 48h to hydrofluoric acid shows the absence of inorganic contaminants. (d) PTFE diffraction pattern reported in the literature. Source: Lebedev (2010).

The diffraction pattern shows the distinctive peaks of PTFE. The most intense peak is located at a 2θ angle of $\sim 18.10^\circ$ and corresponds to the crystalline phase of PTFE. The peaks of the amorphous phase are located at $\sim 40^\circ$. The data and the diffraction pattern obtained were compared with pure PTFE analysis previously reported in the literature.⁹⁵ Furthermore, **Figure (3.2)** shows the distinct diffraction patterns obtained before and after exposing the sample to hydrofluoric acid for different times. This suggests that the purification process depends on the exposure time of the PTFE sample to hydrofluoric acid. In this sense, a 24h exposure shows the rutile phase of titanium dioxide in the diffraction pattern. However, after 48h, the contaminant is completely eliminated.

Interplanar Distances

Bragg's law was used to calculate the distance between the crystallographic planes of PTFE. The calculations were performed using Origin Pro software, transforming the degrees of the peaks into radians.

$$n \lambda = 2d \sin(\theta) \quad (2.1)$$

Where:

- n = integer number known as order of reflection. In this case, it equals 0.94.
- λ = X-ray wavelength
- d = distance between crystalline planes
- θ = Bragg's angle at which the peak is observed

Solving for d :

$$d = \frac{n\lambda}{2 \sin \theta}$$

$$d = \frac{1 * 0.15406}{2 \sin 0.158170463} = 0.4890 \text{ nm}$$

The interplanar distances (d-spacing) calculated for PTFE are shown in **Table 3.1**. Miller indices for PTFE peaks were compared with the ones reported in the literature to determine the correct planes for each intense peak. The obtained values of d-spacing and 2θ degrees perfectly match the ones from previously published data.⁹⁶

Table 3.1. Miller indices, interplanar distances, and peak location calculated from XRD pattern.

| (hkl) | d-spacing (nm) | 2θ (°) |
|--------------|-----------------------|---------------------------------|
| (100) | 0.4890 | 18.1250 |
| (110) | 0.2827 | 31.6165 |
| (107) | 0,2432 | 36.922 |
| (108) | 0,2242 | 40.1870 |
| (210) | 0,1852 | 49.1280 |

Crystal Geometry Equation for Hexagonal Lattice

Taking into account the fact PTFE has a hexagonal crystal structure¹ and the data of table 3.1, the lattice parameters were computed using the following equation.

$$\frac{1}{d^2} = \frac{4}{3} \left(\frac{h^2 + hk + k^2}{a^2} \right) + \frac{l^2}{c^2} \quad (3.6)$$

In the equation above, **h**, **k**, **l**, and **d** are known parameters. However, variables **a** and **c** are unknown. For this reason, the plane (100) and its corresponding d-spacing are chosen to calculate the lattice parameter **a**.

$$\frac{1}{0.489042811^2} = \frac{4}{3} \left(\frac{1^2 + 1 \cdot 0 + 0^2}{a^2} \right) + \frac{0^2}{c^2}$$

Solving for a:

$$a = \sqrt{\frac{4 * 0.489042811^2}{3}} = 0.5647nm$$

Once the lattice parameter **a** has been calculated, using the plane (107) and its corresponding d - spacing, the lattice parameter **c** is calculated.

$$\frac{1}{0.243256997^2} = \frac{4}{3} \left(\frac{1^2 + 1.0 + 0^2}{a^2} \right) + \frac{7^2}{c^2}$$

Solving for c:

$$c = \sqrt{\frac{49 * 4 * 0.243256997^2}{3 * 0.5647^2}} = 3.4819nm$$

The calculated unit cell parameters ($a = b = 0.5647$ nm) are highly consistent with the results previously reported in the literature.^{1,97} PTFE presents a hexagonal lattice composed of atoms in helical conformation from 13 atoms / 180-degree turn to 15 atoms/turn and symmetry of 15₇^{1,98} (**Figure 3.3**). Moreover, the hexagonal lattice is defined by two equal coplanar axes at 90° and a third at 120°. These axis systems are defined as follows:

$$a = b \neq c, \alpha = \beta = 90^\circ, \gamma = 120^\circ$$

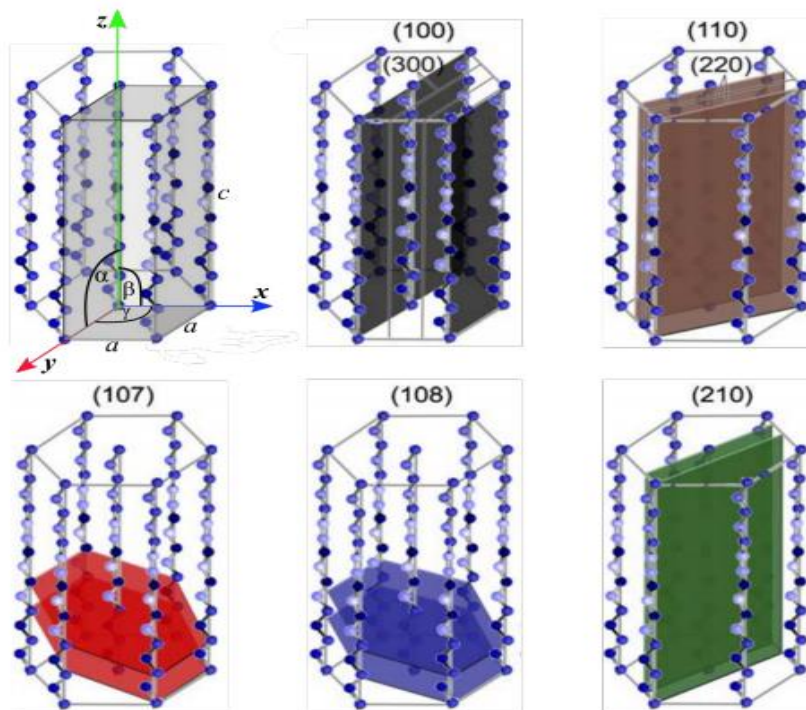


Figure 3.3. Unit cell and diffraction planes of PTFE. The crystalline structure reflects an hexagonal lattice arrangement. Source: Brown, et.al. (2008).

Index of Crystallinity

The diffraction pattern of PTFE is characterized by a high-intensity peak belonging to the crystalline phase at $2\theta - 18.10^\circ$ with a d-spacing of 0.4890 nm. Around $2\theta \sim 40^\circ$, there are some lower intensity dispersion curves (peaks) characteristic of amorphous phases. To summarize, PTFE has a crystalline phase located at $\sim 18.10^\circ$ and two amorphous phases at $\sim 40^\circ$.⁹⁵ To calculate the index of crystallinity (IC), the crystalline phase peak area was deconvoluted using OriginPro Software and subsequently divided with the total area of the diffraction pattern (amorphous phases + crystalline phase).

$$IC = \frac{\text{Area of Crystalline Peaks}}{\text{Total Area (Crystalline + Amorphous)}} * 100 \quad (3.7)$$

$$IC = \frac{265822.9406}{312896.165} * 100 = 85 \%$$

Crystallite Size

The Scherrer equation estimates the crystallite size by relating the width to the height of the half peak of a diffraction pattern.⁹⁹ The mathematical expression is defined as follows:

$$l = \frac{k \lambda}{B \cos \theta} \quad (3.8)$$

Where:

- **B** = Full width at a half maximum (FWHM)
- λ = X-ray wavelength (0.15406 nm)
- θ = Diffraction angle
- **K** = Numerical constant equal to 0.94.

It is essential to consider that the value of FWHM is directly related to the crystallite size. Therefore, the higher the FWHM value, the smaller the crystallite size. To estimate the crystallite size, the calculation of full-width values at half maximum was carried out using the Origin Pro software applying the Levenberg Marquardt algorithm for fitting curves. **Table 3.2** shows the calculated values of full width at a half maximum together with the values of 2θ and θ .

Table 3.2. Values of full-width at a half maximum calculated from the PTFE X-ray diffraction pattern.

| Peak Position (2θ , °) | θ (°) | FWHM |
|-----------------------------------|--------------|--------|
| 18,1250 | 9,0625 | 0,2672 |
| 31,6166 | 15,8083 | 0,3703 |
| 36,922 | 18,4611 | 0,8014 |
| 40,1870 | 20,0935 | 8,6659 |
| 49,1280 | 24,564 | 1,0368 |

Applying the Scherrer equation with the data in Table 3.5, it is possible to determine the crystallite size for each of the peaks present in the diffraction pattern.

Solving for l :

$$l = \frac{0.90 * 0.15406}{0.26724 \cos 9.0625} = 30.129 \text{ nm}$$

The particle size result obtained by the Scherrer equation is not directly related to the TEM and SEM microscopy results. The Scherrer equation has several sources of uncertainty which contribute to the variation of the crystallite size¹⁰⁰ (**Figure 3.4**).

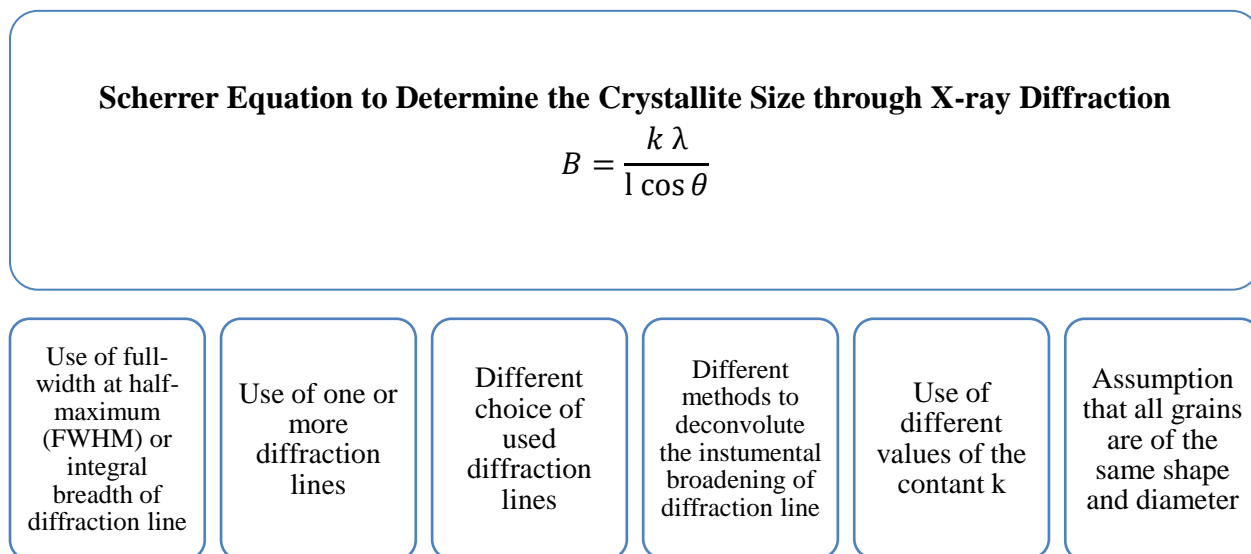


Figure 3.4. Factors that influence the Scherrer equation to calculate the crystallite size utilizing the X-ray diffraction pattern.

To conclude, Table 3.3 summarizes all the parameters calculated from the diffraction pattern. Here is included peak positions, characteristics of the unit cell, crystallite size, and interplanar distance.

Table 3.3. Summary of the parameters calculated from the PTFE diffraction pattern.

| Miller Indices | Unit Cell Parameters (nm) | | | 2θ (°) | FWHM (°) | D-spacing | Crystallite Size (nm) |
|----------------|---------------------------|--------|--------|---------------|----------|-----------|-----------------------|
| | a | b | c | | | | |
| (100) | | | | 18.1250 | 0.2672 | 0.4890 | 30,1029 |
| (110) | | | | 31.6165 | 0.3703 | 0.2827 | 22,2975 |
| (107) | 0.5647 | 0.5647 | 3.4819 | 36.922 | 0.8014 | 0,2432 | 10,4501 |
| (108) | | | | 40.1870 | 8.6659 | 0,2242 | 0,9761 |
| (210) | | | | 49.1280 | 1.0368 | 0,1853 | 8,4242 |

3.1.3 X-ray Photoelectron Spectroscopy (XPS)

XPS analysis of PTFE was carried out using a VERSAPROBE PHI 5000 spectrometer equipped with a 180 hemispherical electron energy analyzer. The X-rays are generated through a monochromatic aluminum $K\alpha$ source with an energy of 1486.6 eV. The survey operation bandpass employs 255 kV and a high-resolution acquisition bandpass at 55 kV with a spot size diameter of 100 μm . OriginPRO software was used to analyze the peaks of F1s, C1s, F2s of the PTFE spectrum and deconvolution of multiple peaks, as seen in **Figure 3.5**.

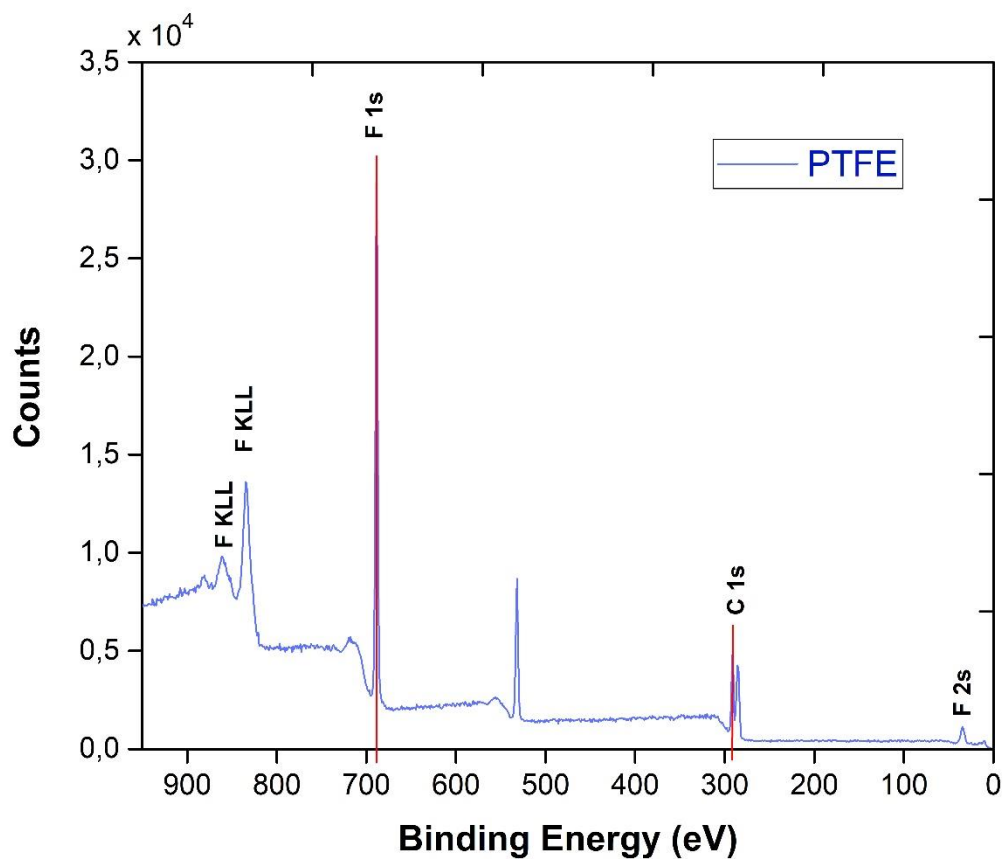


Figure 3.5. XPS survey spectrum of PTFE. The most intense peak is attributed to F1s (685.0 eV), while the less intense peaks are assigned to O1s (530.0 eV) and C1s (284.8 eV). This wide scan survey reveals the O1s atom as the sole contaminant. There is no significant evidence of contamination with inorganic elements.

The spectroscopy pattern was compared with the literature to identify the position of the peaks of the atoms that make up the pure PTFE sample and validate the results. In the XPS spectrum, the characteristic peaks of fluorine and carbon can be recognized (**Figure 3.5**). The total percentage of carbon and fluorine is 85.5%. However, oxygen is also present in the sample (14.3%).

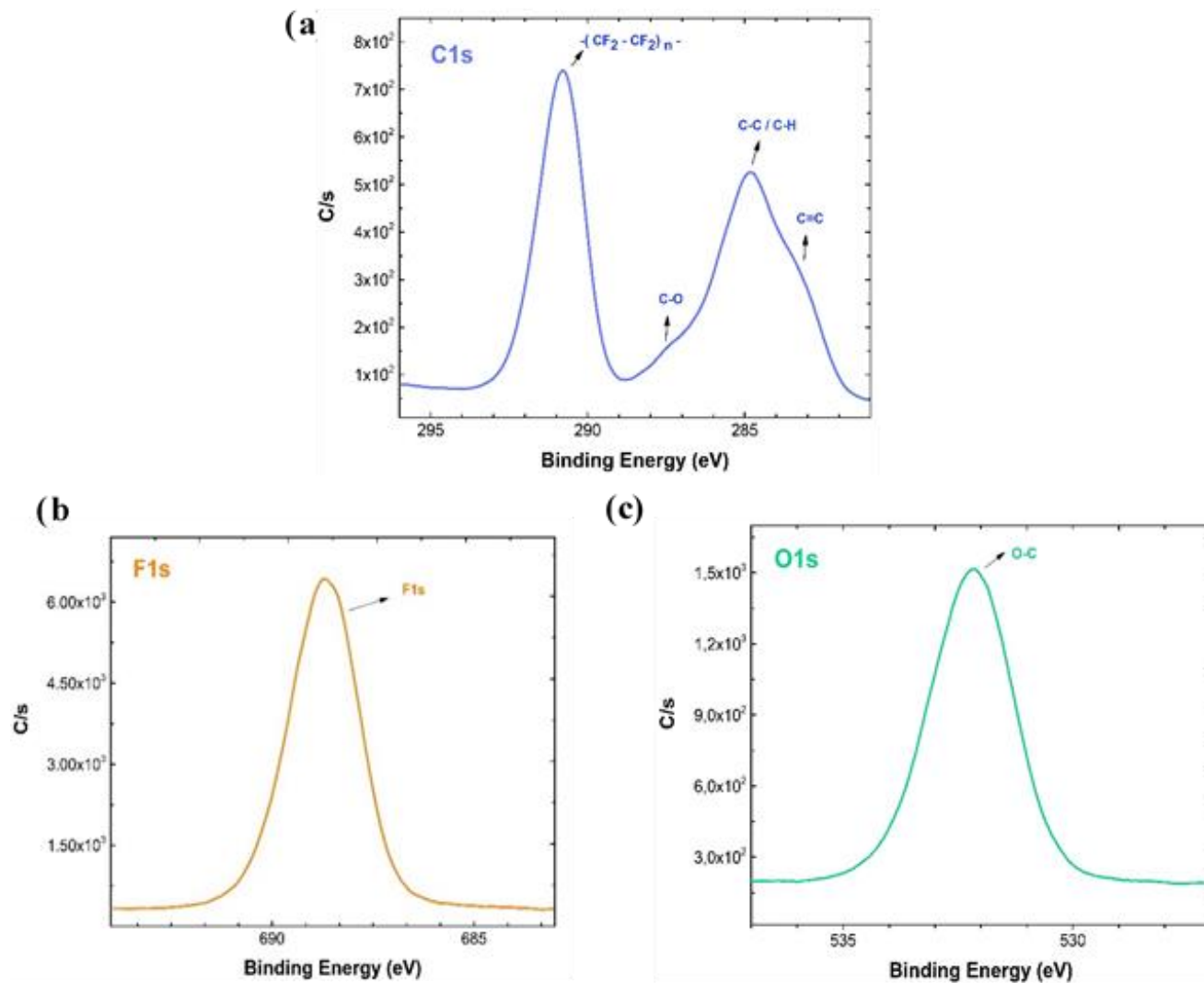


Figure 3.6. High-resolution survey spectrum and peak deconvolution of PTFE.

The XPS spectrum data processing allowed the identification of the different components of the C1s photoelectron peaks (**Figure 3.6**). The spectrum was calibrated at a binding energy of 284.8 eV attributed to C-C/C-H. Therefore, the C1s peak is deconvoluted into three main peaks corresponding to C-O (286.5 eV), CF_2 (291.0 eV) and C=C (~283.8 eV). Similarly, the deconvolution of the F1s peak revealed a binding energy of 688.7 eV belonging to the CF_2 chemical bond. These results fit perfectly with previously published work.¹⁰¹⁻¹⁰³

Finally, **Table 3.4** shows the results obtained from the deconvolution of the F1s, C1s and O1s peaks. The presence of oxygen might be attributed to O₂ adsorbed from the air or water during the PTFE preparation process from the sealant or in the synthesis of PTFE fine-powder and nanoparticles. There is also the possibility that these oxygen atoms result from the alcohol groups of the solvent used in the synthesis process of PTFE nanoparticles (ethanol). Regarding C, the presence of C=C bonds on the PTFE carbon backbone might result from an incomplete polymerization process of TFE.

Table 3.4. Atomic percentage and binding energies of the elements that compose PTFE.

| Element | Percentage (%) | Components | Binding Energy (eV) |
|---------|----------------|------------------------|---------------------|
| C1s | 42.2 | <u>C=C</u> | 283.8 |
| | | <u>C-C/C-H</u> | 284.8 |
| | | <u>C-O</u> | 286.5 |
| | | <u>C-F₂</u> | 291.0 |
| F1s | 43.2 | <u>C-F₂</u> | 688.7 |
| O1s | 14.3 | O-C | 532.2 |

3.1.4 Transmission Electron Microscopy (TEM - PTFE NPS)

The transmission electron microscopy micrographs in **Figures 3.7** a, b and c show the morphology of the PTFE nanoparticles. In fact, it is easy to recognize a miscellaneous population of nanoparticles with spherical and rod shapes in a range of 10 to 160 nm (Figure 3.7).

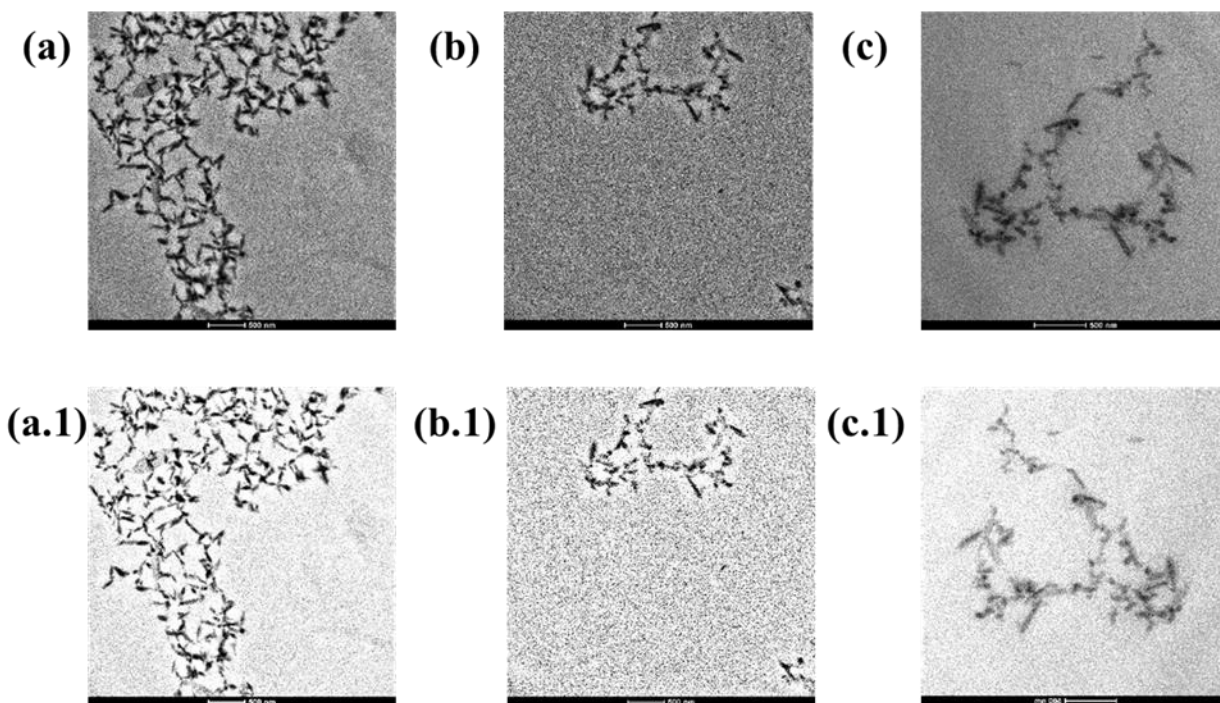


Figure 3.7. Transmission electron Microscopy micrograph of PTFE NPs. The obtained images display spherical and rod morphologies.

As seen in **Figure 3.8** the TEM images were fitted using OriginPro and ImageJ software to estimate the normal distribution of the nanoparticles' average diameter size, giving a result of ~ 70 nm.

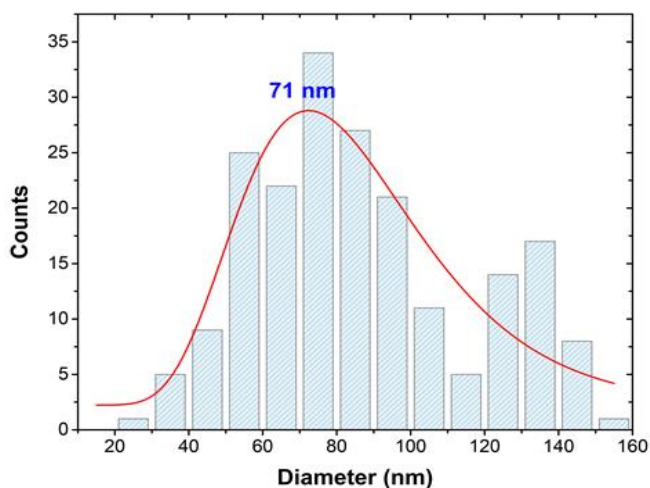


Figure 3.8. Particle size distribution. The histogram displays PTFE NPs ranging from 30 nm to 150 nm with an average diameter of 70 nm.

For bioimaging applications, the size of the nanoparticles is diverse. In this case, these PTFE nanoparticles fit perfectly within the range of polymeric nanoparticles that can be conjugated with other elements for bioimaging purposes.^{104,105} For subsequent work, it is necessary to optimize the ultrasound exposure parameters to generate a homogeneous population of nanoparticles.

CHAPTER 4

CONCLUSIONS & OUTLOOK

4.1 Conclusion

Nowadays, several X-ray and ultrasound-assisted bioimaging nanoplatforms have been developed for the early detection and efficient treatment of cancer. Therefore, this work highlights the relevance of scientific research in biomedicine applied to early cancer detection, especially in developing nanoparticles as the synthesized nanomaterials of interest are obtained from low-cost, commercially available products. The synthesis of PTFE from low-cost commercial products is a promising alternative that will permit a more detailed investigation of PTFE applications. In this sense, the synthesis of PTFE nanoparticles was carried out by readjusting the protocol developed in our Research Group to eliminate contaminating entities. The PTFE-fine powder sample was subjected to various concentrations of different acids to eliminate impurities, hydrofluoric acid being the substance that reduced contamination with TiO_2 . The outcomes revealed that the elimination of TiO_2 is directly proportional to the exposure time of the PTFE sample to hydrofluoric acid. This process made it possible to verify the material's chemical stability by removing only the contaminating substances and not altering the chemical composition of the PTFE.

Likewise, the XPS analysis confirmed the absence of contaminant inorganic substances. The deconvolution of the high-resolution spectra demonstrated the presence of the chemical bonds of CF_2 , CF , C-C , and C=C in addition to the O1s peak. Finally, the images acquired by transmission electron microscopy (TEM) revealed the spherical and rod morphologies together with the size (30-150 nm) of the PTFE and an average size of 70 nm. However, some particle agglomerations were also visible, these could be avoided by optimizing the ultrasound system's parameters to obtain a homogeneous nanoparticles population.

4.2 Outlook

The main objective of this project was to synthesize Teflon-like nanoparticles, their characterization and application in biomedicine. This thesis demonstrates that PTFE can be

obtained from cheap commercial products. Furthermore, the literature reports that PTFE is an extremely versatile and highly biocompatible material when it interacts with the human body. Immediate follow-ups of this work involve performing biocompatibility analysis of the PTFE nanoparticles to validate their safety and the absence of any adverse effects to the human body. First, their cytotoxicity will be studied using human cell cultures before studying their biocompatibility using animal models. Then, it is planned to investigate the PTFE attenuation of X-ray and ultrasound irradiations at distinct frequencies to be implemented as a contrast agent for bioimaging. The surface chemistry of this material and its pharmacokinetics features will be explored. The exploitation of nanoscaled PTFE in the biomedical field is at its early infancy. There is no doubt it will witness tremendous developments in the coming years owing to its outstanding physico-chemical and biological properties.

APPENDIX**A1 Abbreviations**

| Notation | Description |
|-----------------|--|
| PTFE | Polytetrafluoroethylene |
| TFE | Tetrafluoroethylene |
| CTAs | Chemical Technical Assistance |
| SOLCA | Sociedad de Lucha Contra el Cáncer |
| INSPI | Instituto Nacional de Investigación en Salud Pública |
| NIR | Near Infrared |
| NSMs | Nanostructured Materials |
| CVD | Chemical Vapor Deposition |
| NPs | Nanoparticles |
| PRINT | Particle Replication In Non Wetting Templates |
| PFPE | Perfluoropolyether |
| PLGA | Poly (Lactic-co-glycolic acid) |
| PLA | Poly (Lactic acid) |
| PCL | Polycaprolactone |
| SERS | Surface Enhanced Raman Spectroscopy |
| Notation | Description |

| | |
|----------|----------------------------------|
| PEI | Polyethylenimine |
| MSCT | Multislice Computed Tomography |
| PVA | Polyvinyl Alcohol |
| UCAs | Ultrasound Contrast Agents |
| WHO | World Health Organization |
| GLOBOCAN | Global Cancer Observatory |
| RT | Room Temperature |
| XRD | X-ray Diffraction |
| SEM | Scanning Electron Microscopy |
| TEM | Transmission Electron Microscopy |

BIBLIOGRAPHY

1. Brown EN, Rae PJ, Dattelbaum DM, Clausen B, Brown DW. In-situ measurement of crystalline lattice strains in polytetrafluoroethylene. *Exp Mech*. 2008;48(1):119–31.
2. Ebnesajjad S. *Expanded PTFE Applications Handbook* [Internet]. 1st editio. Norwich, United States: William Andrew; 2016. Available from:
<https://www.sciencedirect.com/book/9781437778557/expanded-ptfe-applications-handbook#book-info>
3. Puts GJ, Crouse P, Ameduri BM. *Polytetrafluoroethylene: Synthesis and Characterization of the Original Extreme Polymer*. *Chem Rev* [Internet]. 2019 [cited 2021 Feb 25]; Available from: <https://pubs.acs.org/doi/abs/10.1021/acs.chemrev.8b00458>
4. Ebnesajjad S. *Manufacturing Polytetrafluoroethylene. Introduction to Fluoropolymers*. 2013. 91–124 p.
5. McKeen LW. *Fluoropolymers*. In: *Film Properties of Plastics and Elastomers* [Internet]. Elsevier; 2012 [cited 2021 Feb 25]. p. 255–313. Available from:
<https://linkinghub.elsevier.com/retrieve/pii/B9781455725519000116>
6. Risbud M V., Hambir S, Jog J, Bhonde R. Biocompatibility assessment of polytetrafluoroethylene/wollastonite composites using endothelial cells and macrophages. *J Biomater Sci Polym Ed* [Internet]. 2001 [cited 2021 Feb 25];12(11):1177–89. Available from: <https://www.tandfonline.com/doi/abs/10.1163/156856201753395734>
7. Stanisławska A. *Biomaterials and Implants in Cardiac and Vascular Surgery - Review*. *Adv Mater Sci* [Internet]. 2015 May 6 [cited 2021 Feb 25];14(3):5–17. Available from:
<https://content.sciendo.com/view/journals/adms/14/3/article-p5.xml>
8. Snyder RW, Helmus MN. *CARDIOVASCULAR BIOMATERIALS*. In: *Standard Handbook of Biomedical Engineering and Design* [Internet]. 2004 [cited 2021 Feb 25].

- Available from: <https://www.accessengineeringlibrary.com/content/book/9780071356374>
9. Xue L, Greisler HP. Biomaterials in the development and future of vascular grafts. *J Vasc Surg.* 2003 Feb 1;37(2):472–80.
 10. Korzinskas T, Jung O, Smeets R, Stojanovic S, Najman S, Glenske K, et al. In vivo analysis of the biocompatibility and macrophage response of a non-resorbable PTFE membrane for guided bone regeneration. *Int J Mol Sci* [Internet]. 2018 Oct 1 [cited 2021 Feb 25];19(10). Available from: <https://pubmed.ncbi.nlm.nih.gov/30262765/>
 11. GORE MEDICAL. GORE-TEX® Vascular Grafts | Gore Medical [Internet]. 2020 [cited 2021 Feb 25]. Available from: <https://www.goremedical.com/products/vg>
 12. Maitz MF. Applications of synthetic polymers in clinical medicine. *Biosurface and Biotribology* [Internet]. 2015;1(3):161–76. Available from: <http://dx.doi.org/10.1016/j.bsbt.2015.08.002>
 13. Elango S, Perumalsamy S, Ramachandran K, Vadodaria K. Mesh materials and hernia repair. *BioMedicine* [Internet]. 2017 Sep 25 [cited 2021 Feb 25];7(3):16. Available from: <http://biomedicine.edp-open.org/10.1051/bmdcn/2017070316>
 14. GORE MEDICAL. GORE-TEX® Soft Tissue Patch | Gore Medical Middle East Africa [Internet]. 2020 [cited 2021 Feb 25]. Available from: <https://www.goremedical.com/me/products/stp>
 15. Dhandayuthapani B, Sakthi kumar D. Biomaterials for Biomedical Applications. In: *Biomedical Applications of Polymeric Materials and Composites* [Internet]. Weinheim, Germany: Wiley-VCH Verlag GmbH & Co. KGaA; 2016 [cited 2021 Feb 25]. p. 1–20. Available from: <http://doi.wiley.com/10.1002/9783527690916.ch1>
 16. Menczel JD. Surgical sutures. In: *Thermal Analysis of Textiles and Fibers* [Internet]. Elsevier; 2020 [cited 2021 Feb 25]. p. 259–70. Available from:

- <https://linkinghub.elsevier.com/retrieve/pii/B978008100572900015X>
17. GORE MEDICAL. GORE-TEX® Suture | Gore Medical [Internet]. 2020 [cited 2021 Feb 25]. Available from: <https://www.goremedical.com/products/suture>
 18. Korgaonkar N, Yadav KS. Understanding the biology and advent of physics of cancer with perspicacity in current treatment therapy. *Life Sci.* 2019 Dec 15;239:117060.
 19. Hassanpour SH, Dehghani M. Review of cancer from perspective of molecular. *J Cancer Res Pract.* 2017 Dec 1;4(4):127–9.
 20. Van Cott C. Cancer Genetics. *Surg Clin North Am* [Internet]. 2020 Jun 1 [cited 2021 Feb 25];100(3):483–98. Available from: <http://www.surgical.theclinics.com/article/S0039610920300256/fulltext>
 21. World Health Organization. Cancer [Internet]. 2018. [cited 2021 Feb 25]. Available from: <https://www.who.int/news-room/fact-sheets/detail/cancer>
 22. GLOBOCAN. Cancer Today [Internet]. 2020 [cited 2021 Feb 25]. Available from: <https://gco.iarc.fr/today/home>
 23. Globocan. Ecuador Source: Globocan 2020. Int Agency Reserch Cancer [Internet]. 2020;563:1–2. Available from: <https://gco.iarc.fr/today/data/factsheets/populations/218-ecuador-fact-sheets.pdf>
 24. Pública M de S. Estrategia Nacional para la Atención Integral del Cancer en el Ecuador [Internet]. Ministerio de Salud Pública. 2017. Available from: https://aplicaciones.msp.gob.ec/salud/archivosdigitales/documentosDirecciones/dnn/archivos/ac_0059_2017.pdf
 25. National Cancer Institute. Surgery for Cancer - National Cancer Institute [Internet]. 2015 [cited 2021 Jun 23]. Available from: <https://www.cancer.gov/about->

- cancer/treatment/types/surgery
26. Oude Vrielink TJC, Vitiello V, Mylonas GP. Robotic surgery in cancer [Internet]. Bioengineering Innovative Solutions for Cancer. Elsevier Ltd.; 2019. 245–269 p. Available from: <http://dx.doi.org/10.1016/B978-0-12-813886-1.00012-7>
 27. National Cancer Institute. Radiation Therapy for Cancer - National Cancer Institute [Internet]. 2019 [cited 2021 Jun 23]. Available from: <https://www.cancer.gov/about-cancer/treatment/types/radiation-therapy>
 28. National Cancer Institute. About Cancer - National Cancer Institute [Internet]. [cited 2021 Feb 25]. Available from: <https://www.cancer.gov/about-cancer>
 29. American Cancer Society. Chemotherapy What It Is, How It Helps [Internet]. 2020 [cited 2021 Feb 26]. Available from: <https://www.cancer.org/content/dam/cancer-org/cancer-control/en/booklets-flyers/chemotherapy-what-it-is-how-it-helps.pdf>
 30. National Cancer Institute. Targeted Therapy for Cancer - National Cancer Institute [Internet]. 2020 [cited 2021 Jun 23]. Available from: <https://www.cancer.gov/about-cancer/treatment/types/targeted-therapies>
 31. National Cancer Institute. Hyperthermia to Treat Cancer - National Cancer Institute [Internet]. 2021 [cited 2021 Jun 23]. Available from: <https://www.cancer.gov/about-cancer/treatment/types/hyperthermia>
 32. Wust P, Hildebrandt B, Sreenivasa G, Rau B, Gellermann J, Riess H, et al. Hyperthermia in combined treatment of cancer. *Lancet Oncol*. 2002;3(8):487–97.
 33. Fratila RM, de la Fuente JM. Introduction to Hyperthermia. *Nanomater Magn Opt Hyperth Appl*. 2018;1–10.
 34. Mallory M, Gogineni E, Jones GC, Greer L, Simone CB. Therapeutic hyperthermia: The

- old, the new, and the upcoming. *Crit Rev Oncol Hematol* [Internet]. 2016;97(2015):56–64. Available from: <http://dx.doi.org/10.1016/j.critrevonc.2015.08.003>
35. Bidram E, Esmacili Y, Ranji-Burachaloo H, Al-Zaubai N, Zarrabi A, Stewart A, et al. A concise review on cancer treatment methods and delivery systems. *J Drug Deliv Sci Technol* [Internet]. 2019;54(July):101350. Available from: <https://doi.org/10.1016/j.jddst.2019.101350>
36. Jiang BP, Zhang L, Guo XL, Shen XC, Wang Y, Zhu Y, et al. Poly(N-phenylglycine)-Based Nanoparticles as Highly Effective and Targeted Near-Infrared Photothermal Therapy/Photodynamic Therapeutic Agents for Malignant Melanoma. *Small*. 2017;13(8):1–15.
37. Leon L, Chung EJ, Rinaldi C. A brief history of nanotechnology and introduction to nanoparticles for biomedical applications [Internet]. *Nanoparticles for Biomedical Applications: Fundamental Concepts, Biological Interactions and Clinical Applications*. Elsevier Inc.; 2019. 1–4 p. Available from: <http://dx.doi.org/10.1016/B978-0-12-816662-8.00001-1>
38. Bhatia S. Natural polymer drug delivery systems: Nanoparticles, plants, and algae. *Natural Polymer Drug Delivery Systems: Nanoparticles, Plants, and Algae*. 2016. 1–225 p.
39. Martin CR. Welcome to Nanomedicine. *Nanomedicine* [Internet]. 2006 [cited 2021 Feb 26];1(1):5–5. Available from: <http://nihroadmap.nih.gov/nanomedicine/>
40. Jha S, Sharma PK, Malviya R. Hyperthermia: Role and Risk Factor for Cancer Treatment. *Achiev Life Sci* [Internet]. 2016;10(2):161–7. Available from: <http://dx.doi.org/10.1016/j.als.2016.11.004>
41. Ngô C, Van de Voorde M. *Nanotechnology in a Nutshell*. Nanotechnology in a Nutshell. Paris: Atlantis Press; 2014.

42. Rafique M, Tahir MB, Rafique MS, Safdar N, Tahir R. Nanostructure materials and their classification by dimensionality. In: *Nanotechnology and Photocatalysis for Environmental Applications*. Elsevier; 2020. p. 27–44.
43. Tiwari JN, Tiwari RN, Kim KS. Zero-dimensional, one-dimensional, two-dimensional and three-dimensional nanostructured materials for advanced electrochemical energy devices. *Prog Mater Sci* [Internet]. 2012;57(4):724–803. Available from: <http://dx.doi.org/10.1016/j.pmatsci.2011.08.003>
44. Khan I, Saeed K, Khan I. Nanoparticles: Properties, applications and toxicities. *Arab J Chem* [Internet]. 2019;12(7):908–31. Available from: <http://dx.doi.org/10.1016/j.arabjc.2017.05.011>
45. Iqbal P, Preece JA, Mendes PM. Nanotechnology: The “Top-Down” and “Bottom-Up” Approaches. *Supramol Chem*. 2012;
46. Gratton SEA, Pohlhaus PD, Lee J, Guo J, Cho MJ, DeSimone JM. Nanofabricated particles for engineered drug therapies: A preliminary biodistribution study of PRINT™ nanoparticles. *J Control Release*. 2007;121(1–2):10–8.
47. Xu J, Wong DHC, Byrne JD, Chen K, Bowerman C, Desimone JM. Future of the particle replication in nonwetting templates (PRINT) technology. *Angew Chemie - Int Ed*. 2013;52(26):6580–9.
48. OpenWetWare. Particles Replication in Non-Wetting Templates - Anh Nguyen - OpenWetWare [Internet]. 2019 [cited 2021 Feb 26]. Available from: https://openwetware.org/wiki/Particles_Replication_in_Non-Wetting_Templates_-_Anh_Nguyen
49. Bhatia S, Bhatia S. Nanoparticles Types, Classification, Characterization, Fabrication Methods and Drug Delivery Applications. In: *Natural Polymer Drug Delivery Systems* [Internet]. Springer International Publishing; 2016 [cited 2021 Feb 26]. p. 33–93.

- Available from: https://link.springer.com/chapter/10.1007/978-3-319-41129-3_2
50. Park JH, Saravanakumar G, Kim K, Kwon IC. Targeted delivery of low molecular drugs using chitosan and its derivatives. *Adv Drug Deliv Rev* [Internet]. 2010;62(1):28–41. Available from: <http://dx.doi.org/10.1016/j.addr.2009.10.003>
 51. Hu Y, Zhi Z, Zhao Q, Wu C, Zhao P, Jiang H, et al. 3D cubic mesoporous silica microsphere as a carrier for poorly soluble drug carvedilol. *Microporous Mesoporous Mater* [Internet]. 2012;147(1):94–101. Available from: <http://dx.doi.org/10.1016/j.micromeso.2011.06.001>
 52. Dang Y, Guan J. Nanoparticle-based drug delivery systems for cancer therapy. *Smart Mater Med* [Internet]. 2020;1(February):10–9. Available from: <https://doi.org/10.1016/j.smaim.2020.04.001>
 53. Sur S, Rathore A, Dave V, Reddy KR, Chouhan RS, Sadhu V. Recent developments in functionalized polymer nanoparticles for efficient drug delivery system. *Nano-Structures and Nano-Objects* [Internet]. 2019;20. Available from: <https://doi.org/10.1016/j.nanoso.2019.100397>
 54. Betof AS, Lascola CD, Weitzel D, Landon C, Scarbrough PM, Devi GR, et al. Modulation of murine breast tumor vascularity, hypoxia, and chemotherapeutic response by exercise. *J Natl Cancer Inst*. 2015;107(5):1–6.
 55. Zhang K, Waxman DJ. Impact of tumor vascularity on responsiveness to antiangiogenesis in a prostate cancer stem cell-derived tumor model. *Mol Cancer Ther* [Internet]. 2013 May 1 [cited 2021 Feb 26];12(5):787–98. Available from: www.aacrjournals.org
 56. Fung AS, Lee C, Yu M, Tannock IF. The effect of chemotherapeutic agents on tumor vasculature in subcutaneous and orthotopic human tumor xenografts. *BMC Cancer*. 2015;15(1):1–10.

57. Di Ianni T, Bose RJC, Sukumar UK, Bachawal S, Wang H, Telichko A, et al. Ultrasound/microbubble-mediated targeted delivery of anticancer microRNA-loaded nanoparticles to deep tissues in pigs. *J Control Release*. 2019;309(February):1–10.
58. Fahmy MD, Jazayeri HE, Razavi M, Hashemi M, Omidi M, Farahani M, et al. *Biomedical Applications of Intelligent Nanomaterials*. *Intell Nanomater Second Ed*. 2017;199–245.
59. Giner-Casares JJ, Henriksen-Lacey M, Coronado-Puchau M, Liz-Marzán LM. Inorganic nanoparticles for biomedicine: Where materials scientists meet medical research. *Mater Today*. 2016;19(1):19–28.
60. Oncology AS of C. ASCO Answers. *Understanding Chemotherapy*. 2014;2015(22 May 2015). Available from:
http://www.cancer.net/sites/cancer.net/files/asco_answers_chemotherapy.pdf
61. Huang S, Chen P, Xu C. Facile preparation of rare-earth based fluorescence/MRI dual-modal nanoprobe for targeted cancer cell imaging. *Talanta [Internet]*. 2017;165(December 2016):161–6. Available from: <http://dx.doi.org/10.1016/j.talanta.2016.12.048>
62. Fu D, Liu D, Zhang L, Sun L. Self-assembled fluorescent tripeptide nanoparticles for bioimaging and drug delivery applications. *Chinese Chem Lett [Internet]*. 2020;31(12):3195–9. Available from: <https://doi.org/10.1016/j.ccllet.2020.07.011>
63. Chang H, Yoo J, Kim H, Park W, Hahn SK, Kwon W. Controlled growth of fluorescent silica nanoparticles using two-phase orthogonal solvents for bioimaging. *J Lumin [Internet]*. 2019;214(June):116529. Available from:
<https://doi.org/10.1016/j.jlumin.2019.116529>
64. Deng H, Huang S, Xu C. Intensely red-emitting luminescent upconversion nanoparticles for deep-tissue multimodal bioimaging. *Talanta [Internet]*. 2018;184(February):461–7. Available from: <https://doi.org/10.1016/j.talanta.2018.03.018>

65. Hahn MA, Singh AK, Sharma P, Brown SC, Moudgil BM. Nanoparticles as contrast agents for in-vivo bioimaging: Current status and future perspectives. *Anal Bioanal Chem.* 2011;399(1):3–27.
66. Speck U. Contrast agents: X-ray contrast agents and molecular imaging - A contradiction? *Handb Exp Pharmacol* [Internet]. 2008 [cited 2021 Feb 26];185(PART1):167–75. Available from: https://link.springer.com/chapter/10.1007/978-3-540-72718-7_8
67. Lusic H, Grinstaff MW. X-ray-computed tomography contrast agents. *Chem Rev.* 2013;113(3):1641–66.
68. Aslan N, Ceylan B, Koç MM, Findik F. Metallic nanoparticles as X-Ray computed tomography (CT) contrast agents: A review. *J Mol Struct* [Internet]. 2020;1219. Available from: <https://doi.org/10.1016/j.molstruc.2020.128599>
69. Habets J, Meijer TS, Meijer RCA, Mali WPTM, Vonken EJPA, Budde RPJ. CT attenuation measurements are valuable to discriminate pledgets used in prosthetic heart valve implantation from paravalvular leakage. *Br J Radiol* [Internet]. 2012 Sep [cited 2021 Feb 27];85(1017):e616. Available from: </pmc/articles/PMC3487076/>
70. Balegamire J, Vandamme M, Chereul E, Si-Mohamed S, Azzouz Maache S, Almouazen E, et al. Iodinated polymer nanoparticles as contrast agent for spectral photon counting computed tomography. *Biomater Sci.* 2020;8(20):5715–28.
71. Klauser AS. Contrast-Enhanced Ultrasound. In: *Essential Applications of Musculoskeletal Ultrasound in Rheumatology* [Internet]. Elsevier; 2010 [cited 2021 Feb 27]. p. 317–26. Available from: <https://linkinghub.elsevier.com/retrieve/pii/B9781437701272100243>
72. Ignee A, Atkinson NSS, Schuessler G, Dietrich CF. Ultrasound contrast agents. *Endosc Ultrasound* [Internet]. 2016 Nov 1 [cited 2021 Feb 27];5(6):355–62. Available from: </pmc/articles/PMC5206822/>

73. Yin T, Wang P, Zheng R, Zheng B, Cheng D, Zhang X, et al. Nanobubbles for enhanced ultrasound imaging of tumors. *Int J Nanomedicine*. 2012;7:895–904.
74. Fu L, Ke H Te. Nanomaterials incorporated ultrasound contrast agents for cancer theranostics. *Cancer Biology and Medicine* [Internet]. 2016 Sep 1 [cited 2021 Feb 27];13(3):313–24. Available from: [/pmc/articles/PMC5069833/](#)
75. Ke H, Wang J, Dai Z, Jin Y, Qu E, Xing Z, et al. Bifunctional gold nanorod-loaded polymeric microcapsules for both contrast-enhanced ultrasound imaging and photothermal therapy. *J Mater Chem*. 2011;21(15):5561–4.
76. Union for International Cancer Control. THE ECONOMICS OF CANCER PREVENTION & CONTROL: DATA DIGEST | ICCP Portal [Internet]. 2014 [cited 2021 Jun 23]. Available from: <https://www.iccp-portal.org/economics-cancer-prevention-control-data-digest>
77. Pan American Health Organization, World Health Organization. PAHO/WHO | Regional Cancer Experts Discuss a New Initiative on Cancer Prevention For Latin America and the Caribbean [Internet]. 2017 [cited 2021 Jun 23]. Available from: https://www3.paho.org/hq/index.php?option=com_content&view=article&id=13203:new-initiative-cancer-prevention-lac&Itemid=42322&lang=en
78. Pradhan S, Hedberg J, Blomberg E, Wold S, Odnevall Wallinder I. Effect of sonication on particle dispersion, administered dose and metal release of non-functionalized, non-inert metal nanoparticles. *J Nanoparticle Res*. 2016;18(9):1–14.
79. Jordens J, Appermont T, Gielen B, Van Gerven T, Braeken L. Sonofragmentation: Effect of Ultrasound Frequency and Power on Particle Breakage. *Cryst Growth Des*. 2016;16(11):6167–77.
80. Rege K, Medintz I. Biodegradable, targeted polymeric nanoparticle drug delivery formulation for cancer therapy. *Methods in Bioengineering*. 2009. 197–235 p.

81. Kusters KA, Pratsinis SE, Thoma SG, Smith DM. Ultrasonic fragmentation of agglomerate powders. *Chem Eng Sci.* 1993;48(24):4119–27.
82. Ladd M, Palmer R. Structure determination by X-ray crystallography: Analysis by X-rays and neutrons. *Structure Determination by X-ray Crystallography: Analysis by X-rays and Neutrons.* Springer US; 2013. 1–756 p.
83. Sima F, Ristoscu C, Duta L, Gallet O, Anselme K, Mihailescu IN. Laser thin films deposition and characterization for biomedical applications [Internet]. *Laser Surface Modification of Biomaterials: Techniques and Applications.* Elsevier Ltd; 2016. 77–125 p. Available from: <http://dx.doi.org/10.1016/B978-0-08-100883-6.00003-4>
84. Singh AK. *Experimental Methodologies for the Characterization of Nanoparticles. Engineered Nanoparticles.* 2016. 125–170 p.
85. Ul-Hamid A. *A Beginners' Guide to Scanning Electron Microscopy. A Beginners' Guide to Scanning Electron Microscopy.* 2018.
86. Ebnesajjad S. *Surface and Material Characterization Techniques. Surface Treatment of Materials for Adhesive Bonding.* 2014. 39–75 p.
87. Das S, Mukherjee A, Sengupta G, Singh VK. Overview of nanomaterials synthesis methods, characterization techniques and effect on seed germination [Internet]. *Nano-Materials as Photocatalysts for Degradation of Environmental Pollutants: Challenges and Possibilities.* Elsevier Inc.; 2020. 371–401 p. Available from: <http://dx.doi.org/10.1016/B978-0-12-818598-8.00018-3>
88. Yesilkir-Baydar S, Oztel ON, Cakir-Koc R, Candayan A. Evaluation techniques [Internet]. *Nanobiomaterials Science, Development and Evaluation.* Elsevier Ltd; 2017. 211–232 p. Available from: <http://dx.doi.org/10.1016/B978-0-08-100963-5.00011-2>
89. Vitha MF. *Spectroscopy: Principles and Instrumentation by Mark F. Vitha [Internet]. 2nd*

- Editio. John Wiley & Sons; 2018 [cited 2021 Feb 27]. Available from:
https://play.google.com/store/books/details/Spectroscopy_Principles_and_Instrumentation?id=v2hvDwAAQBAJ&hl=en_IE
90. Wang H, Chu PK. Surface Characterization of Biomaterials [Internet]. Characterization of Biomaterials. Elsevier; 2013. 105–174 p. Available from: <http://dx.doi.org/10.1016/B978-0-12-415800-9.00004-8>
 91. Engelhard MH, Droubay TC, Du Y. X-ray photoelectron spectroscopy applications. *Encycl Spectrosc Spectrom*. 2016;716–24.
 92. Welker RW. Size Analysis and Identification of Particles [Internet]. Vol. 4, Developments in Surface Contamination and Cleaning: Detection, Characterization, and Analysis of Contaminants. Elsevier; 2012. 179–213 p. Available from: <http://dx.doi.org/10.1016/B978-1-4377-7883-0.00004-3>
 93. Baer DR, Thevuthasan S. Characterization of Thin Films and Coatings [Internet]. Third Edit. Handbook of Deposition Technologies for Films and Coatings. Elsevier Ltd.; 2010. 749–864 p. Available from: <http://dx.doi.org/10.1016/B978-0-8155-2031-3.00016-8>
 94. Bock S, Kijatkin C, Berben D, Imlau M. Absorption and remission characterization of pure, dielectric (nano-)powders using diffuse reflectance spectroscopy: An end-to-end instruction. *Appl Sci*. 2019;9(22).
 95. Lebedev YA, Korolev YM, Polikarpov VM, Ignat'ev LN, Antipov EM. X-Ray powder diffraction study of polytetrafluoroethylene. *Crystallogr Reports*. 2010;55(4):609–14.
 96. Bouzник VM, Kirik SD, Solovyov LA, Tsvetnikov AK. A crystal structure of ultra-dispersed form of polytetrafluoroethylene based on X-ray powder diffraction data. *Powder Diffr*. 2004;19(3):219–24.
 97. Bunn CW, Howells ER. Structures of molecules and crystals of fluoro-carbons. *Nature*.

- 1954;174(4429):549–51.
98. Clark ES. The crystal structure of polytetrafluoroethylene, forms I and IV. *J Macromol Sci - Phys.* 2006;45 B(2):201–13.
99. Heck RM, Farrauto RJ, Gulati ST. Catalyst Characterization. In: *Catalytic Air Pollution Control* [Internet]. Hoboken, NJ, USA: John Wiley & Sons, Inc.; 2012 [cited 2021 Feb 27]. p. 41–62. Available from: <http://doi.wiley.com/10.1002/9781118397749.ch3>
100. Tomaszewski PE. The uncertainty in the grain size calculation from X-ray diffraction data. *Phase Transitions.* 2013;86(2–3):260–6.
101. Vandecasteele N, Reniers F. Plasma-modified polymer surfaces: Characterization using XPS. *J Electron Spectrosc Relat Phenomena* [Internet]. 2010;178–179(C):394–408. Available from: <http://dx.doi.org/10.1016/j.elspec.2009.12.003>
102. Agraharam S, Hess DW, Kohl PA, Bidstrup Allen SA. Plasma chemistry in fluorocarbon film deposition from pentafluoroethane/argon mixtures. *J Vac Sci Technol A Vacuum, Surfaces, Film.* 1999;17(6):3265–71.
103. Takeishi S, Kudo H, Shinohara R, Hoshino M, Fukuyama S, Yamaguchi J, et al. Plasma-Enhanced Chemical Vapor Deposition of Fluorocarbon Films with High Thermal Resistance and Low Dielectric Constants. *J Electrochem Soc.* 1997;144(5):1797–802.
104. Zielinska A, Carreiró F, Oliveira AM, Neves A, Pires B, Nagasamy Venkatesh D, et al. Polymeric Nanoparticles: Production, Characterization, Toxicology and Ecotoxicology [Internet]. Vol. 25, *Molecules*. MDPI AG; 2020 [cited 2021 Mar 4]. Available from: </pmc/articles/PMC7464532/>
105. Braeken Y, Cheruku S, Ethirajan A, Maes W. Conjugated polymer nanoparticles for bioimaging. *Materials (Basel).* 2017;10(12):1–23.

